Cell Reports

Article

Heme Oxygenase-1 Induction by Blood-Feeding Arthropods Controls Skin Inflammation and Promotes Disease Tolerance

Graphical Abstract

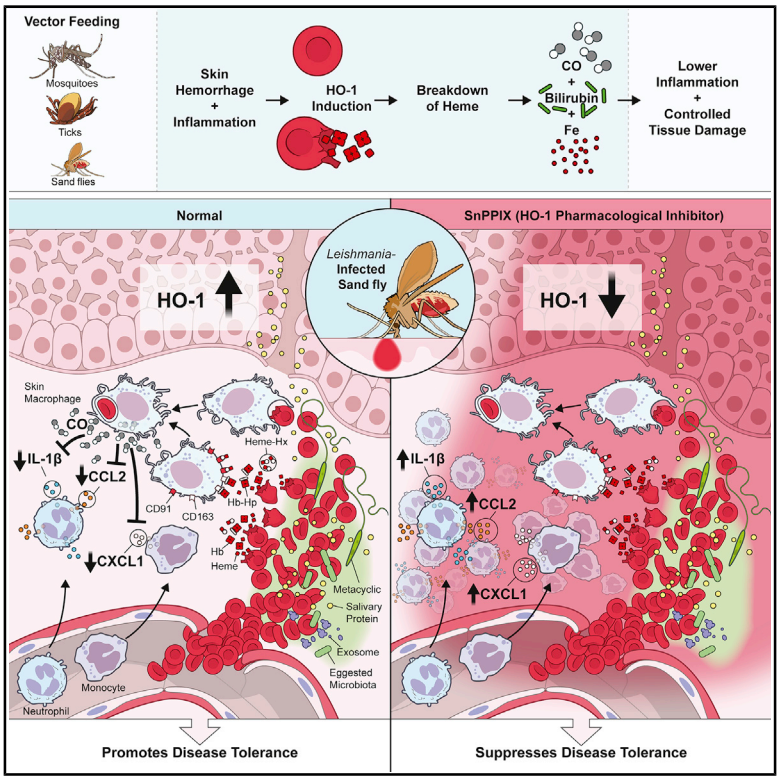

Highlights

- Blood-feeding arthropod bites damage blood vessels, causing RBC leakage into tissue
- Extravascular RBCs are ingested by skin macrophages, leading to production of HO-1
- Inhibition of HO-1 enhances inflammation and promotes tissue damage
- HO-1 production after *Leishmania*-infected sand fly bites promotes disease tolerance

Authors

Thiago DeSouza-Vieira, Eva Iniguez, Tiago D. Serafim, ..., Fabiano Oliveira, Jesus G. Valenzuela, Shaden Kamhawi

Correspondence

jvalenzuela@niaid.nih.gov (J.G.V.), skamhawi@niaid.nih.gov (S.K.)

In Brief

Vector-borne diseases afflict millions of people worldwide. DeSouza-Vieira et al. demonstrate that blood-feeding arthropods induce HO-1 in skin macrophages that ingest extravascular erythrocytes from damaged vessels. Without HO-1, sand fly transmission of *Leishmania* led to aggravated cutaneous leishmaniasis pathology without affecting the parasites, indicating that HO-1 production promotes disease tolerance.

DeSouza-Vieira et al., 2020, Cell Reports *33*, 108317
October 27, 2020
https://doi.org/10.1016/j.celrep.2020.108317

CellPress

Cell Reports

CellPress
OPEN ACCESS

Article

Heme Oxygenase-1 Induction by Blood-Feeding Arthropods Controls Skin Inflammation and Promotes Disease Tolerance

Thiago DeSouza-Vieira,[1,6] Eva Iniguez,[1,6] Tiago D. Serafim,[1] Waldionê de Castro,[1] Subir Karmakar,[2] Maria M. Disotuar,[1] Pedro Cecilio,[1] Joshua R. Lacsina,[1] Claudio Meneses,[1] Bianca M. Nagata,[3] Silvia Cardoso,[4] Daniel E. Sonenshine,[1] Ian N. Moore,[3] Valeria M. Borges,[5] Ranadhir Dey,[2] Miguel P. Soares,[4] Hira L. Nakhasi,[2] Fabiano Oliveira,[1] Jesus G. Valenzuela,[1,*] and Shaden Kamhawi[1,7,*]

[1]Vector Molecular Biology Section, Laboratory of Malaria and Vector Research, National Institute of Allergy and Infectious Diseases, National Institutes of Health, Rockville, MD 20852, USA

[2]Laboratory of Emerging Pathogens, Division of Emerging and Transfusion Transmitted Diseases, Center for Biologics Evaluation and Research, Food and Drug Administration, Silver Spring, MD 20993, USA

[3]Infectious Disease Pathogenesis Section, Comparative Medicine Branch, National Institute of Allergy and Infectious Diseases, National Institutes of Health, Rockville, MD 20852, USA

[4]Instituto Gulbenkian de Ciência, Oeiras, Lisboa 2780-156, Portugal

[5]Gonçalo Moniz Institute, Oswaldo Cruz Foundation, Salvador, Bahia 40296-710, Brazil

[6]These authors contributed equally

[7]Lead Contact

*Correspondence: jvalenzuela@niaid.nih.gov (J.G.V.), skamhawi@niaid.nih.gov (S.K.)

https://doi.org/10.1016/j.celrep.2020.108317

SUMMARY

Hematophagous vectors lacerate host skin and capillaries to acquire a blood meal, resulting in leakage of red blood cells (RBCs) and inflammation. Here, we show that heme oxygenase-1 (HO-1), a pleiotropic cytoprotective isoenzyme that mitigates heme-mediated tissue damage, is induced after bites of sand flies, mosquitoes, and ticks. Further, we demonstrate that erythrophagocytosis by macrophages, including a skin-residing $CD163^{+}CD91^{+}$ professional iron-recycling subpopulation, produces HO-1 after bites. Importantly, we establish that global deletion or transient inhibition of HO-1 in mice increases inflammation and pathology following *Leishmania*-infected sand fly bites without affecting parasite number, whereas CO, an end product of the HO-1 enzymatic reaction, suppresses skin inflammation. This indicates that HO-1 induction by blood-feeding sand flies promotes tolerance to *Leishmania* infection. Collectively, our data demonstrate that HO-1 induction through erythrophagocytosis is a universal mechanism that regulates skin inflammation following blood feeding by arthropods, thus promoting early-stage disease tolerance to vector-borne pathogens.

INTRODUCTION

According to the World Health Organization, more than half the world's population is at risk of contracting a vector-borne disease, and collectively, vector-borne diseases cause more than 700,000 deaths annually (https://www.who.int/news-room/fact-sheets/detail/vector-borne-diseases). Hematophagous arthropods, such as mosquitoes, ticks, and sand flies, are major vectors of human diseases (Franklinos et al., 2019; Shaw and Catteruccia, 2019). During a blood meal, these vectors transmit multiple pathogens, such as *Plasmodium spp.* and arboviruses by mosquitoes (Simões et al., 2018), *Borrelia* by ticks (Mason et al., 2014), and phleboviruses, *Bartonella spp.* and *Leishmania spp.* by sand flies (Ready, 2013), among many others.

The concept of blood-feeding arthropods as "flying needles" that simply inject pathogens has been refuted by a variety of experimental systems. For example, regurgitation of vector-derived factors present in the sand fly inoculum, such as saliva (Belkaid et al., 1998; Titus and Ribeiro, 1988), exosomes (Atayde et al., 2015), and proteophosphoglycans (Giraud et al., 2018), have been shown to orchestrate a complex host inflammatory immune response that favors *Leishmania* parasite survival and replication, leading to disease exacerbation. More recently, our group demonstrated that gut microbiota egested by the sand fly following transmission of *L. donovani* by *Lutzomyia longipalpis* triggers inflammasome activation in neutrophils and drives autocrine amplification of their recruitment through interleukin-1B (IL-1B), sanctioning parasite dissemination to visceral organs (Dey et al., 2018). Hence, vector-derived molecules are critical for *Leishmania* establishment. Similarly, transmission and dissemination of viruses were also enhanced by bites and saliva of mosquitoes (Pingen et al., 2017; Sun et al., 2020), reinforcing the importance of vector-derived factors in modulating the infectivity of vector-borne pathogens.

To obtain a blood meal, blood-feeding arthropods breach the skin and lacerate capillaries and blood vessels, leading to

extravascular leakage of red blood cells (RBCs) and inflammation (Lavoipierre, 1965). Under inflammatory conditions, oxidative stress promotes release of free heme from oxidized hemoproteins, such as hemoglobin (Hb), eliciting the production of free radicals (Gozzelino et al., 2010). Heme oxygenase (HO)-1 is a stress-responsive enzyme that catabolizes the rate-limiting reaction of heme degradation, generating equimolar amounts of Fe, carbon monoxide (CO), and biliverdin (Gozzelino et al., 2010; Singh et al., 2018). Its enzymatic activity has broad cytoprotective and immunoregulatory effects targeting a plethora of genes involved in stress responses (Otterbein et al., 2003). A growing body of evidence has demonstrated that HO-1 affords protection against diseases, such as hepatitis B (Protzer et al., 2007), tuberculosis (Costa et al., 2016; Silva-Gomes et al., 2013), sepsis (Larsen et al., 2010), and malaria (Ferreira et al., 2011). The mechanisms governing these protective effects are pleiotropic (Silva et al., 2020) and rely, to a large extent, on the cytoprotective and immunoregulatory effects of CO (Motterlini and Otterbein, 2010).

In skin, heme oxygenases are cytoprotective against reactive oxygen species generated during normal physiological processes, and they limit oxidative stress following exposure to environmental assaults (Szabo et al., 2018). Previously, we have demonstrated that bites of *L. longipalpis* sand flies induce NFE2L2-dependent production of HO-1 in human skin that was attributed to the effect of saliva (Luz et al., 2018). Here, we show another facet to HO-1 induction in skin triggered by blood-feeding arthropods. We demonstrate that HO-1 is induced following bites of sand flies, mosquitoes, and ticks. Further, we use sand flies to demonstrate that HO-1 is produced by resident and inflammatory macrophages that uptake and digest extravascular RBCs or their constituents, potentially to mitigate the release of heme from Hb upon oxidation (Pamplona et al., 2007). We also show that global deletion of HO-1 or transient pharmacologic inhibition of its activity promotes tolerance to CL after transmission of *Leishmania* parasites by sand flies. We then establish that transient inhibition of HO-1 activity results in increased gene expression of inflammatory mediators, including *CXCL1*, *CXCL2*, *IL-1B*, and chitinase-like 3 (*CHI3L1*). Conversely, local delivery of CO, an end product of heme degradation by HO-1, into tissue dampens the acute inflammatory response. Hence, we establish that HO-1 induction is a universal response to vector bites triggered by extravascular blood, where it suppresses the host inflammatory response via CO, shielding transmitted pathogens at their most vulnerable.

RESULTS

Production of HO-1 in Host Skin Is a Universal Response to Bites of Hematophagous Arthropods

To explore the induction of HO-1 in skin after bites from major arthropod vectors of disease, we exposed mice ears to 10 *L. longipalpis* or *Phlebotomus duboscqi* sand flies, 10 *Aedes aegypti* or *Anopheles gambiae* mosquitoes, or three *Ornithodoros turicata* ticks. Next, we measured HO-1 levels in skin tissue lysates (STLs) by immunoblotting and ELISA at 6 h, 24 h, 48 h, and 1 week after exposure (Figures 1A–1C). Compared to resting skin, HO-1 levels were significantly higher for all tested arthropod vectors with a peak expression at 24 h or 48 h after bites (Figures 1A–1C). In comparison, mechanical damage caused by needle poking resulted in a weak induction of HO-1 (Figures 1A–1C).

To obtain a meal, blood-feeding arthropods breach the skin, lacerate capillaries, and inoculate saliva containing vasodilators and anti-coagulants into host skin (Ribeiro, 1995). We hypothesized that, after vector bites, extravascular leakage of RBCs in the skin might cause hemolysis and potentially Hb release. Accordingly, quantification of total Hb in STL showed a significant increase in its levels compared to unbitten controls at 6 h after bites of all tested arthropod vectors, apart from *A. gambiae*, whose bites resulted in the weakest tissue hemorrhage (Figure 1D). Interestingly, elevated levels of Hb were maintained up to 48 h after *L. Longipalpis* bites (Figure 1D). This may be due to the potency of maxadilan, the vasodilator in saliva (Lerner et al., 1991; Svensjö et al., 2009, 2012), which facilitates blood flow into the bite site. The extensive leakage of RBCs in ear tissue, visible at 6 h and 18 h after sand fly bites, provides further evidence that bleeding drives HO-1 induction at arthropod bite sites (Figure 1E). Similar to what was observed for HO-1 induction, the increase in Hb levels after mechanical damage caused by needle poking was not comparable to vector bites (Figure 1D). Of note, tissue homeostasis was restored at 1 week after bites for all tested arthropod vectors (Figures 1A–1D).

Recently, we published that *L. longipalpis* saliva induces a NFE2L2-dependent production of HO-1 at the site of the bite (Luz et al., 2018). To investigate the contribution of saliva to HO-1 induction at vector bite sites, we compared the intradermal injection of saliva to bites of *Lutzomyia* sand flies and *Aedes* mosquitoes (Figure 1F). Previous studies established that a pair of sand fly salivary glands contains about 0.38–3.00 μg of protein and that a sand fly deposits about 26%–71% of its saliva after feeding (Prates et al., 2008; Ribeiro et al., 1989). Similarly, the protein content in mosquito saliva ranges from 1 to 3 μg per pair of glands and a mosquito deposits about 20%–50% of its saliva into the host (Calvo et al., 2006; Martin-Martin et al., 2020). Based on these data, we injected 1 μg or 3 μg (Figure 1F). Bites or injection of 3 μg of saliva from both insects induced significantly higher levels of HO-1 compared to naive skin (Figure 1F), supporting participation of saliva in HO-1 induction at the bite site. Altogether, these data demonstrate that induction of HO-1 is a universal host skin response to blood-feeding arthropods.

Erythrophagocytosis Triggers HO-1 Production at the Bite Site

Next, we wanted to establish the cellular mechanism by which blood-feeding arthropods induce HO-1 in the skin at the bite site. Fluorescence-activated cell sorting (FACS) analysis of single-cell suspensions obtained from mouse ears 18 h after sand fly bites demonstrates the transient emergence of a population of $CD11b^+$ myeloid cells positive for TER-119, a transmembrane marker exclusive to RBCs (Figure 2A). On average, a 3.5- and a 5-fold increase in the number of $CD11b^+$TER-119^+ cells was observed for *L. longipalpis* and *P. duboscqi*, respectively, compared to unbitten ears (Figures 2B and 2C). Back gating $CD11b^+$TER-119^+ cells onto Ly6G and Ly6C scatterplots

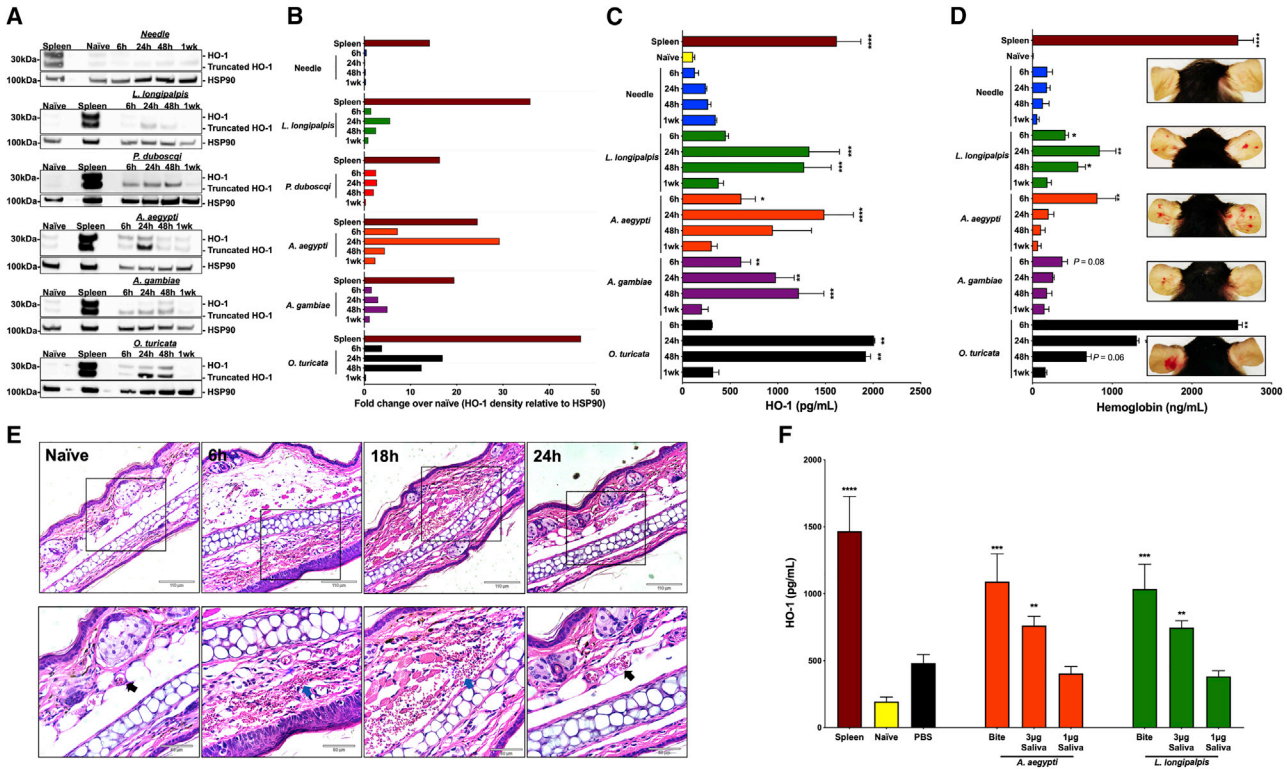

Figure 1. HO-1 Is Induced in Host Skin in Response to Blood-Feeding Arthropod Vectors

(A–D) Skin tissue lysate (STL) of ears exposed to 10 *Lutzomyia longipalpis* or *Phlebotomus duboscqi* sand flies, 10 *Aedes aegypti* or *Anopheles gambiae* mosquitoes, 3 *Ornithodoros turicata* ticks, or poked 10 times with a 32-gauge needle. Naive, unbitten ears, negative control; spleen, positive control.

(A) HO-1 western blot (n = 4–6 pooled ears).

(B) Fold change over naive of HO-1 density relative to the loading control HSP90 for the western blot shown in (A).

(C and D) HO-1 (C) or hemoglobin (D) levels by ELISA. Insets (D) depict hemorrhage (n = 2–6 pooled ears).

(E) H&E stain of skin after 20 *P. duboscqi* bites showing vascular (black arrows) or extravascular (blue arrows) RBCs. Scale bars, 110 μm or 50 μm (n = 4 ears/experiment).

(F) HO-1 levels in ear STL after exposure to 5 *L. longipalpis* or *A. aegypti* bites or intradermal (i.d.) injection of saliva from each insect (n = 4 pooled ears).

Representative blots (A) or images from 2–4 experiments (E). Graphs represent mean ± SEM of cumulative data from 2–4 experiments (C, D, and F). *p ≤ 0.05, **p ≤ 0.01, ***p ≤ 0.001, and ****p ≤ 0.0001; Kruskal-Wallis with Dunn's post hoc analysis (C, D, and F).

determined that the majority of erythrophagocytic cells at the site of the bite are resident myeloid ($Ly6C^{neg}Ly6G^{neg}$) or inflammatory cells ($Ly6C^{int\text{-}high}Ly6G^{neg}$) and did not include neutrophils ($CD11b^{+}Ly6C^{int}Ly6G^{high}$; Figures 2D and 2E). We have previously demonstrated that resident macrophages are a main source of HO-1 at bite sites of *L. longipalpis* (Luz et al., 2018). To better define the type of cells performing erythrophagocytosis, we further distinguished inflammatory from tissue-resident macrophages based on F4/80 and Ly6C expression (Epelman et al., 2014; Leid et al., 2016; Yang et al., 2019). We established that the $CD11b^{+}TER\text{-}119^{+}$ population is composed of a combination of tissue-resident macrophages ($CD11b^{+}F4/80^{+}Ly6C^{neg}Ly6G^{neg}$) and macrophages originating from recruited inflammatory monocytes ($CD11b^{+}F4/80^{+}Ly6C^{high}Ly6G^{neg}$; Figures 2D and 2E). There is evidence that heme originating from erythrocytes influences the phenotype of monocytes, converting them into iron-recycling macrophages (Alam et al., 2017), further supporting our findings. In summary, our data reveal that both tissue and inflammatory macrophages participate in erythrophagocytosis at the bite site.

In the spleen, liver, and bone marrow, aged or damaged erythrocytes are phagocytosed by macrophages that express high levels of HO-1 and are dedicated to recycling iron and amino acids to support bone marrow erythropoiesis (Soares and Hamza, 2016). These specialized macrophages express CD163, a Hb scavenger receptor that mediates the uptake of haptoglobin-Hb complexes (Thomsen et al., 2013), and CD91, which mediates phagocytosis of apoptotic/damaged RBCs and heme-hemopexin complexes (Nilsson et al., 2012; Park and Kim, 2017; Vandivier et al., 2002). Remarkably, we detected a subpopulation of macrophages expressing high levels of CD163 and CD91 in resting skin (Figure 2F). Surprisingly, the number of $CD91^{+}CD163^{+}$ macrophages only marginally increased by 18 h after sand fly bites (Figure 2F). Moreover, only 38.0% of $CD11b^{+}F4/80^{+}TER\text{-}119^{+}$ macrophages were $CD91^{+}CD163^{+}$, and this percentage was similar in $CD11b{+}F4/80^{+}TER\text{-}119^{-}$ (Figure 2G). This suggests that $CD91^{+}CD163^{+}$ macrophages represent only a proportion of the participating erythrophagocytes at the bite site. Collectively, these data demonstrate that macrophages phagocytose RBCs, leading to

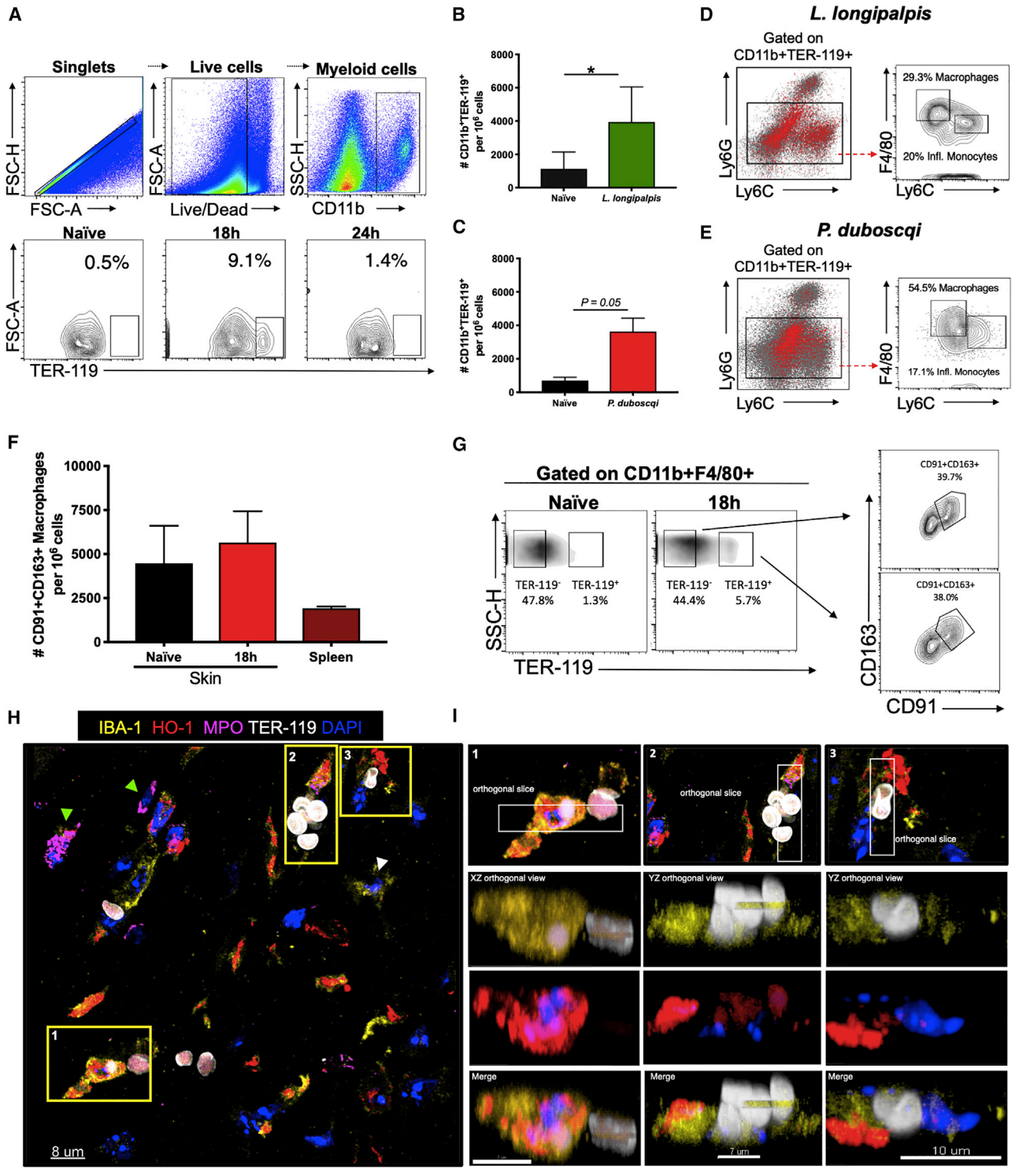

Figure 2. Erythrophagocytosis at the Bite Site Is Carried out by a Specialized Subset of CD91$^+$CD163$^+$ Iron-Recycling Macrophages in Host Skin

(A–G) Mice ear cells recovered after exposure to 20 sand flies.

(A) Gating strategy (top panel) to define CD11b$^+$TER-119$^+$ cells (bottom panel).

(B–I) At 18 h post-bite.

(B and C) Number of CD11b$^+$TER-119$^+$ cells.

(legend continued on next page)

induction of HO-1. Further, they reveal a skin-resident specialized subpopulation of macrophages expressing high levels of CD163 and CD91 that participate in erythrophagocytosis and work as professional iron-recycling erythrophagocytes.

To further validate the occurrence of erythrophagocytosis after vector bites, we visualized it *in situ*. We exposed mouse ears to sand fly bites and obtained skin sections for immunolabeling after 18 h, the peak of erythrophagocytosis based on our flow cytometry observations (Figures 2A–2C). Confocal images show that macrophages (IBA-1$^+$) expressing high levels of HO-1 (HO-1$^+$) have internalized RBCs (TER-119$^+$; Figure 2H). In contrast, neutrophils did not express HO-1 (green arrows), confirming our previous observations (Luz et al., 2018). A white arrow points to a macrophage that has not taken up an RBC and is not expressing HO-1 (Figure 2H). An orthogonal view of z stacks (Figure 2I) and a representative tridimensional reconstruction (Figure S1) confirm the subcellular localization of erythrocytes inside the cytoplasm of HO-1$^+$ macrophages.

HO-1 Promotes Disease Tolerance to Cutaneous Leishmaniasis Transmitted by *L. major*-Infected *Phlebotomus duboscqi* Sand Flies

Next, we questioned whether the induction of HO-1 at the bite site of a blood-feeding vector would influence the pathology of a vector-borne disease. To address this question, we used an infection model of cutaneous leishmaniasis (CL) transmitted by bites of *L. major*-infected *P. duboscqi* sand flies that is well established in our laboratory. To infect sand flies, we fed them a blood meal containing 1 to 2 × 10^6 parasites/mL. For experiments involving follow-up of disease pathology, a subsequent uninfected blood meal was provided to promote a homogeneous transmissible infection (Serafim et al., 2018). The infection status and feeding behavior of infected sand flies used throughout this work are shown in Figure S2.

As the feeding behavior of infected sand flies is distinct from that of uninfected sand flies (Rogers and Bates, 2007), we first established that HO-1 is induced in wild-type (Figures 3A and 3B) and *HMOX1*$^{lox/lox}$ mice (Figure 3C) and verified the presence of extravascular RBCs in the skin of mice ears (Figure S3A) after bites of *L. major*-infected *P. duboscqi* sand flies. We then assessed CL pathology in *HMOX1*$^{R26\Delta/\Delta}$ (Figure S3B) and *HMOX1*$^{lox/lox}$ mice following parasite transmission (Figures 3D–3F). Disease progression, determined by measuring the diameter of developing lesions, was significantly enhanced in *HMOX1*$^{R26\Delta/\Delta}$ mice compared to *HMOX1*$^{lox/lox}$ mice throughout the course of infection (Figure 3E), demonstrating that absence of HO-1 leads to an increase in CL pathology. Interestingly, the observed increase in disease pathology was not reflected by an increase in parasite burden, assessed at week 5 post-transmission (Figures 3F and S3C). As *HMOX1*$^{R26\Delta/\Delta}$ mice did not express HO-1 throughout the course of infection, we wanted to establish whether blocking the effect of its transient induction by blood-feeding arthropods, in the early stages following pathogen deposition and onset of the host inflammatory response, would still have a marked impact on disease pathology long term. To transiently inhibit HO-1 activity *in vivo*, wild-type mice were treated with tin protoporphyrin (SnPPIX), a selective inhibitor of HO-1 activity (Costa et al., 2016), the day prior to, the day of, and the day after vector transmission with *L. major*-infected *P. duboscqi* (Figure 3G). Similar to the outcome of infection in *HMOX1*$^{R26\Delta/\Delta}$ mice, treatment with SnPPIX significantly increased CL pathology compared to PBS-treated animals up to 4 weeks post-transmission, the end point of the experiment, without decreasing the parasite burden (Figures 3H and 3I). This indicates that a transient induction of HO-1 after sand fly bites ameliorates disease pathology but does not control the infection. Controlling CL pathology without affecting *Leishmania* parasites in both *HMOX1*$^{R26\Delta/\Delta}$ and SnPPIX-treated mice demonstrates that HO-1 promotes the establishment of disease tolerance to leishmaniasis.

Next, we wanted to investigate the mechanism by which HO-1 promotes the establishment of disease tolerance to leishmaniasis. Because HO-1 exerts a potent anti-inflammatory effect under distinct pathological and physiological scenarios (Martins et al., 2019; Medzhitov et al., 2012; Vanella et al., 2016), we hypothesized that HO-1 induction at the bite site may regulate the acute inflammatory burst observed in the skin after infected sand fly bites (Dey et al., 2018). To explore this hypothesis, we performed a targeted transcriptional analysis of genes involved in inflammation and the cell stress response by quantitative RT-PCR (Figure 3J). Compared to PBS-injected animals, treatment with SnPPIX resulted in dysregulation of the inflammatory response characterized by increased gene expression of *IL-1B* and *CHI3L1*, which promote neutrophil infiltration (Dey et al., 2018; Sutherland et al., 2014), as well as *CXCL1* and *CXCL2* chemokines involved in neutrophil and inflammatory monocyte infiltration, respectively (Paudel et al., 2019; Shi and Pamer, 2011), at 18 h after infected bites (Figures 3J and 3K). A significant increase in expression of *HMOX1* and the iron export protein Ferroportin-1 (*SLC40A1*) genes was also observed (Figures 3J and 3K), potentially due to heme and Fe accumulation, respectively, in macrophages.

HO-1 Regulates Inflammation at the Bite Site by Modulating Tissue Infiltration by Neutrophils and Inflammatory Monocytes

We next verified the nature of the inflammatory response after *L. major*-infected *P. duboscqi* sand flies. Similar to

(D and E) Ly6G and Ly6C expression on CD11b$^+$TER-119$^+$ cells and F4/80 expression on Ly6G^{neg} cells.
(F–I) Exposed to *P. duboscqi* bites.
(F) Number of CD11b$^+$F4/80$^+$CD91$^+$CD163$^+$ macrophages.
(G) CD91 and CD163 expression on TER-119$^+$ versus TER-119$^-$ macrophages. Naive, unbitten ears; spleen, positive control.
(H) Skin section immunolabeled with IBA-1 (macrophages), HO-1 (HO-1), myeloperoxidase (MPO) (neutrophils), TER-119 (RBCs), and DAPI (nuclei). Yellow squares, macrophages internalizing RBCs; green arrowheads, neutrophils; white arrowhead, a resting macrophage.
(I) Orthogonal slicing of (G) projected in 2D. Scale bars, 7 μm, 8 μm, or 10 μm.
Representative plots (A, D, E, and G) or images (H and I) from 2 experiments. Graphs represent mean ± SEM of cumulative data of 4 pooled ears/experiment with 1–3 replicates (B) and 1 to 2 replicates (C and F) from 2 to 3 experiments. *p ≤ 0.05; Mann-Whitney *U*-test (B and C) or Kruskal-Wallis with Dunn's post hoc analysis (F). See also Figure S1.

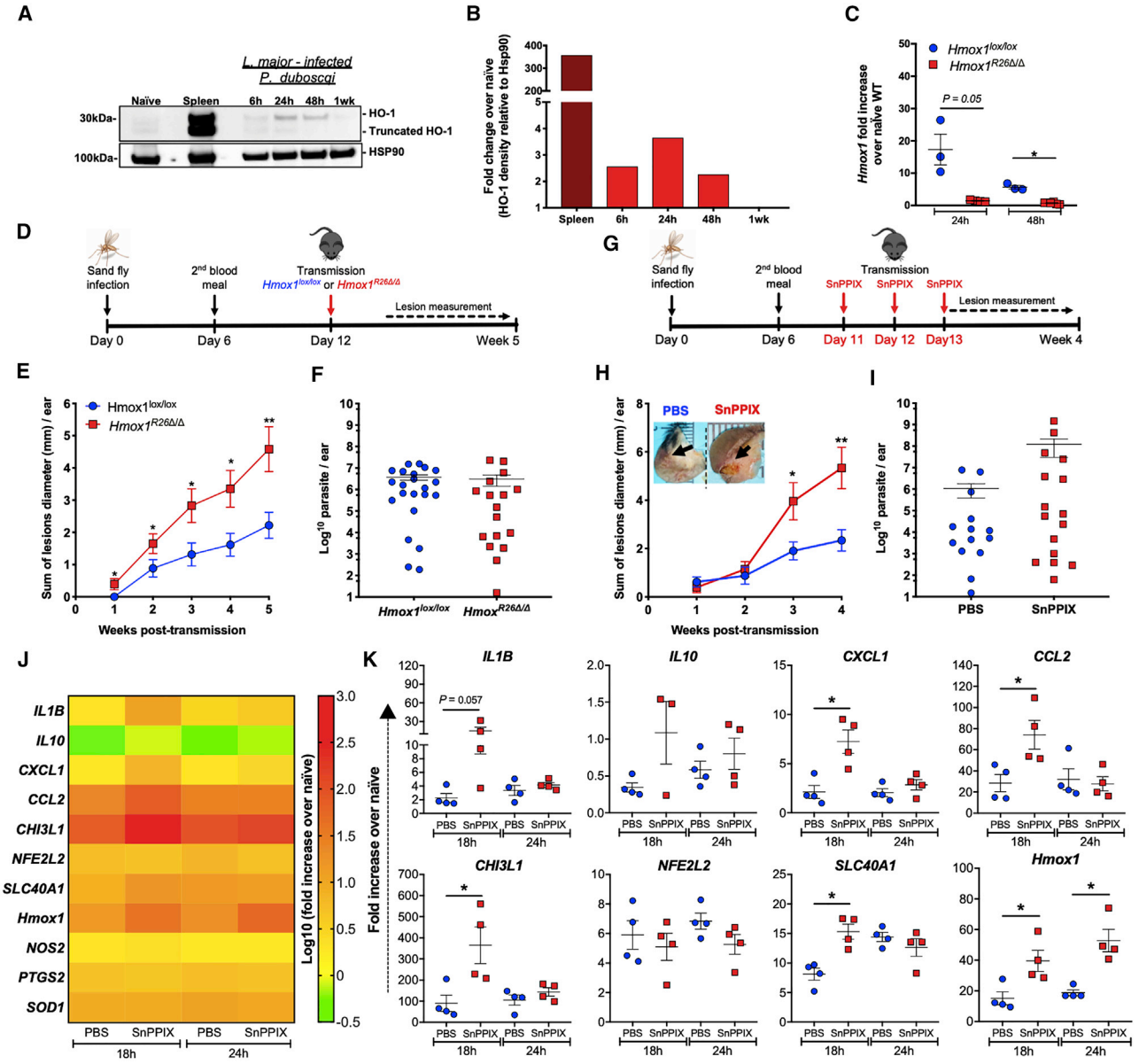

Figure 3. HO-1 Promotes Disease Tolerance to *Leishmania major* Infection

(A–K) Mice ears exposed to 10 (E–I) or 20 (A–C, J, and K) *L. major*-infected *P. duboscqi.* The ear tissue was lysed at the indicated time points after vector bites.

(A) HO-1 western blot from skin tissue lysate (STL) (n = 2–4 pooled ears).

(B) Fold change over naive of HO-1 density relative to the loading control HSP90 for the western blot shown in (A).

(C) mRNA expression of *HMOX1* transcript in *HMOX1*$^{lox/lox}$ and *HMOX1*$^{R26\Delta/\Delta}$ mice by quantitative RT-PCR (n = 3–6 ears).

(D–F) Transmission to *HMOX1*$^{lox/lox}$ and *HMOX1*$^{R26\Delta/\Delta}$ mice (n = 8–12 ears).

(D) Experimental design.

(E) Sum of lesions diameter.

(F) Parasite load per ear at week 5 post-transmission.

(G–I) Transmission to SnPPIX-treated mice (n = 4–10 ears).

(G) Experimental design.

(H) Sum of lesions diameter. Black arrows indicate cutaneous lesions 4 weeks post-transmission.

(I) Parasite load per ear at week 4 post-transmission.

(J) mRNA expression of inflammatory mediators in SnPPIX-treated mice post-transmission (n = 4 ears). Scale bar, log10 (fold change over naive).

(K) Expression profile of transcripts modulated by HO-1 inhibition.

Representative western blot from 2 experiments (A and B). Graphs represent mean ± SEM. Cumulative data (E, F, H, and I) and representative data (J and K) from 2 experiments are shown. A single experiment was conducted for (C). *p $\leq$ 0.05 and **p $\leq$ 0.01; Mann-Whitney *U*-test (C, E, F, H, I, and K). See also Figures S2 and S3 and Table S1.

L. donovani-infected *L. longipalpis* bites (Dey et al., 2018), we observed an intense infiltration of $CD11b^{+}Ly6C^{int}Ly6G^{high}$ neutrophils at 6 h post-bite followed by a progressive infiltration of $CD11b^{+}Ly6C^{high}Ly6G^{neg}$ inflammatory monocytes (Figures 4A and 4B). Moreover, neutrophils accounted for 70% of the IL-$1B^{+}$ cells infiltrating the tissue at 6 h after sand fly bites (Figures 4A and 4B). Coincidental to the induction of HO-1, IL-1B production decreased sharply by 24–48 h, despite a progressive infiltration of leukocytes. Accordingly, compared to controls, HO-1 inhibition by SnPPIX treatment significantly increased the infiltration of neutrophils and monocytes at 24 h after infected sand fly bites (Figures 4C and 4D). Additionally, pharmacological inhibition of HO-1 *in vivo* also increased the mean fluorescence intensity of CD11b on neutrophils compared to PBS-injected animals, 24 h after infected bites (Figure 4E), suggestive of their higher state of activation (Keeney et al., 1993). For $HMOX1^{R26\Delta/\Delta}$ compared to $HMOX1^{lox/lox}$ mice, infiltration of $CD11b^{+}$ cells, including monocytes and $CD11b^{+}$IL-$1B^{+}$ cells, was also increased at 48 h after *L. major*-infected *P. duboscqi* bite (Figure S4). However, the effect was not pronounced particularly for neutrophils (Figure S4C), potentially due to the overall neutrophilia reported for $HMOX1^{R26\Delta/\Delta}$ mice (Devey et al., 2009).

CO is one of the end products of heme degradation by HO-1 and is a bioactive gasotransmitter that suppresses inflammation (Pamplona et al., 2007). To test whether HO-1 exerts its anti-inflammatory effect through CO, we injected CO releasing molecule 2 (CORM-2) intradermally into mice ears. Administration of CORM-2 2 h after vector transmission (Figure 4F) did not reduce the number of neutrophils infiltrating the ear (Figure 4G) but resulted in a 60% decrease in the relative number of neutrophils secreting IL-1B (Figure 4H). Collectively, these data provide evidence that the production of HO-1 in the skin dampens the acute inflammatory response induced by infected sand fly bites through the anti-inflammatory properties of its end products, including CO.

DISCUSSION

The majority of arthropod vectors transmit pathogens during blood feeding, yet the implication of RBC release into surrounding tissue after vascular damage has been overlooked to date. Our current findings demonstrate that the bleeding caused by arthropod bites, potentiated by anti-hemostatic molecules in vector saliva, is a universal and critical event that shapes the initial host inflammatory response to vector-borne pathogens. Extravascular RBCs, and potentially Hb and heme constituents, are internalized by resident and inflammatory macrophages, leading to the induction of HO-1 in the skin, where pathogens are deposited after bites by infected arthropod vectors.

Clearance of RBCs is necessary to restore hemostasis and prevent heme-mediated tissue damage from oxidized Hb (Pamplona et al., 2007; Schaer et al., 2013). Restoration of hemostasis after skin injury is attributed to the host wound response and coagulation (Martin, 1997; Nurden, 2011; Opneja et al., 2019), and several studies have associated cutaneous HO-1 induction with accelerated wound healing (Brogliato et al., 2014; Grochot-Przeczek et al., 2009). High levels of HO-1 after vector bites contrasted with its poor induction following mechanical damage caused by a needle. This is potentially due to anti-hemostatic factors egested by hematophagous arthropods to facilitate blood feeding by promoting enhanced extravasation of RBCs into the skin. These factors likely intensify HO-1 induction and may potentially lead to accelerated wound healing after arthropod bites, emphasizing yet another facet to the complexity of the effect of arthropod bites on the local innate immune response of the host.

Our data suggest that induction of HO-1 at the bite site of *Leishmania*-infected sand flies promotes disease tolerance to CL. Tolerance is a defense strategy that controls pathogen-mediated damage rather than the infection itself (Martins et al., 2019; Medzhitov et al., 2012). The involvement of HO-1 in promoting disease tolerance has been described for several infections, including sepsis (Larsen et al., 2010) and malaria (Ferreira et al., 2011). For malaria, another vector-borne disease transmitted by *Anopheles* mosquitoes, HO-1 promoted initial stages of liver infection (Epiphanio et al., 2008) but conferred protection against severe disease thereafter (Martins et al., 2019; Pamplona et al., 2007). HO-1 also protected *Leishmania* parasites and promoted their persistence during visceral leishmaniasis (Luz et al., 2012; Saha et al., 2019). These studies, however, focused mostly on the role of HO-1 when a disease has been established. We now propose that HO-1 induction at the bite site by blood-feeding vectors may play an equally important part in regulating inflammation during early stages of infection, thus impacting disease progression.

For CL, the effect of transient inhibition of HO-1 on disease exacerbation was evident up to 5 weeks post-infection, despite the fact that HO-1 levels in the skin subside within 24–48 h after vector bites. This suggests that early induction of HO-1 may alter the nature of the inflammatory response long term. Of note, because HO-1 induction after infected sand fly bites had a significant effect on dampening inflammation, we cannot preclude an early benefit to *Leishmania* parasites. However, as HO-1 induction is transient, the low number of transmitted parasites combined with their logarithmic growth likely limits any significant advantage to the parasites. Though this study is focused on CL, the effect of HO-1 induction at the bite site of other arthropod vectors of disease needs to be evaluated for each pathogen, particularly for those involving dissemination to distal organs.

Here, we identify the presence of $CD11b^{+}F4/80^{+}CD91^{+}$ $CD163^{+}$ iron-recycling resident macrophages in skin that engulf RBCs and induce HO-1 production after vector bites. Their presence in steady-state skin demonstrates that $CD163^{+}CD91^{+}$ erythrophagocytes reside in skin and can promptly internalize extravascular RBCs. Though we only establish the occurrence of erythrophagocytosis in this study, constituents such as free hemoglobin or heme released from damaged or lysed RBCs may also be taken up directly via CD163. Indeed, senescent and damaged RBCs are cleared from the bloodstream by a similar subset of $CD163^{+}CD91^{+}$ macrophages in the spleen, liver, and bone marrow (Alam et al., 2017; Nairz et al., 2017). Surprisingly, this population did not seem to expand after the inflammatory insult caused by sand fly bites. We propose that some of these macrophages may have shed CD163 and CD91 on their surface. It has been reported that activation of microglia by lipopolysaccharide or calreticulin stimulates shedding of CD91

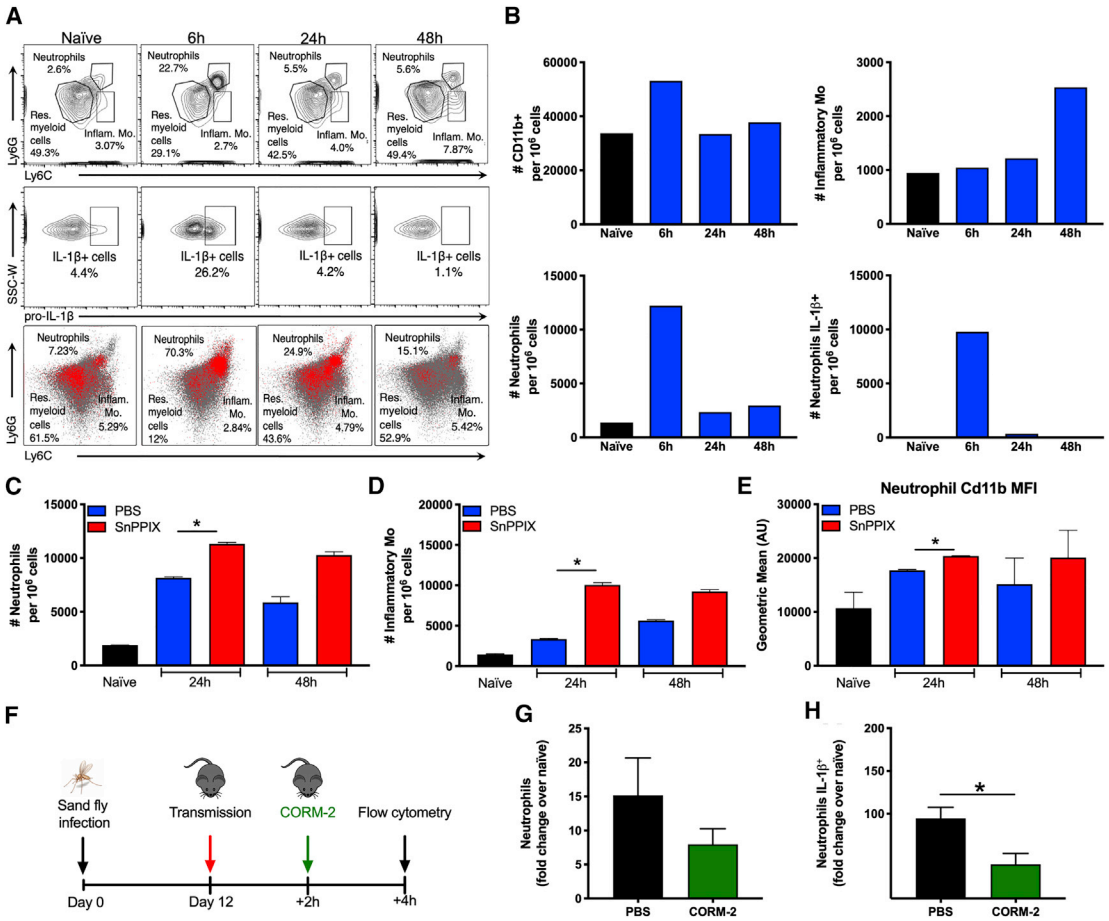

Figure 4. HO-1 Regulates Inflammation at the Bite Site by Modulating Tissue Infiltration by Neutrophils and Inflammatory Monocytes

(A–H) Mice ears exposed to 20 *L. major*-infected *P. duboscqi* sand flies.

(A–E) Inflammatory infiltrate in mice ears.

(A) Percentage of neutrophils, inflammatory monocytes (inflam. mo.), and resident myeloid cells (res. myeloid cells) (top panel); $CD11b^+IL\text{-}1B^+$ cells (middle panel); Ly6G and Ly6C expression on $CD11b^+IL\text{-}1B^+$ cells (bottom panel).

(B) Number of $CD11b^+$ cells, inflammatory monocytes, neutrophils, and $IL\text{-}1B^+$ neutrophils. n = 4–6 pooled mice ears for (A) and (B).

(C–E) Transmission to SnPPIX-treated or PBS-injected mice. Number of neutrophils (C) and inflammatory monocytes (D) in mice ears and mean fluorescent intensity (MFI) of CD11b on neutrophils (E) are shown. n = 4–6 pooled ears per replicate with 1–4 replicates/experiment.

(F–H) Transmission to mice ears injected i.d. with CORM-2 or PBS.

(F) Experimental design.

(G) Total neutrophil number.

(H) Number of $IL\text{-}1B^+$ neutrophils. n = 4–6 pooled mice ears.

Representative plots (A) or cumulative data (B) of 2 experiments. Graphs represent mean ± SEM. Representative data from 3 (C and D) or 2 (E) experiments are shown. Cumulative data (G and H) from 5 experiments are shown. *$p \leq 0.05$; Mann-Whitney *U*-test (C–E, G, and H). See also Figures S2 and S4.

(Brifault et al., 2017), although CD163 expression in monocytes and macrophages is suppressed by lipopolysaccharide, interferon (IFN)-γ and tumor necrosis factor alpha (TNF-α) (Buechler et al., 2000). Hence, the magnitude of $CD163^+CD91^+$ macrophages participating in the inflammatory environment created after vector bites may be underestimated in this study. Our data indicate that other macrophage subsets, including monocyte-derived macrophages, also phagocytose RBCs following sand-fly-mediated vascular damage. An in-depth genomic characterization is needed to better elucidate the nature of the remaining macrophage subsets and their involvement in erythrophagocytosis and HO-1 induction in skin after vector bites. Moreover, whether an increase in temperature due to the acute inflammatory conditions at the bite site contributes to the induction of HO-1, a heat shock protein, should also be determined.

Injecting CORM-2 at the time of *Leishmania* transmission enabled us to demonstrate that CO decreases the percent of $IL\text{-}1B^+$ neutrophils. We have previously established that IL-1B promotes the continued infiltration of neutrophils to the bite site (Dey et al., 2018). Our present data extend this observation, demonstrating that HO-1 induction may be a central mechanism in controlling acute inflammation resulting from bites of blood-feeding arthropods. IL-1B production by neutrophils after infected sand fly bites is mediated by gut microbes that activate

the NLRP3 inflammasome (Dey et al., 2018). It is possible that CO and other anti-inflammatory byproducts of the HO-1 reaction may reduce IL-1B production by directly inhibiting cell inflammasomes. A recent study of experimental autoimmune encephalomyelitis demonstrated that IL-1R1 signaling suppresses HO-1 expression by blood brain barrier endothelial cells, revealing a direct antagonistic association between HO-1 and IL-1 (Hauptmann et al., 2020). More studies are needed to elucidate how CO and other byproducts of the HO-1 reaction exert their well-established anti-inflammatory effect on cells and whether dampening the inflammatory response will have a long-term effect on the development of the adaptive immune response.

Collectively, our study reveals a universal mechanism triggered by blood-feeding arthropods that regulates inflammation at the bite site of disease vectors with broad implications for pathogenesis of vector-borne disease.

STAR★METHODS

Detailed methods are provided in the online version of this paper and include the following:

- KEY RESOURCES TABLE
- RESOURCE AVAILABILITY
  - Lead contact
  - Materials availability
  - Data and code availability
- EXPERIMENTAL MODEL AND SUBJECT DETAILS
  - Mice
  - Parasites
  - Sand flies, mosquitoes, and ticks rearing
- METHOD DETAILS
  - Sand fly infection
  - Salivary gland homogenate
  - Mice exposure to vector bites or needle pokes
  - Immunoblotting and ELISA immunosorbent assays
  - Immunohistochemistry and confocal microscopy
  - SnPPIX and CORM-2 treatment
  - Cytokine determination by quantitative RT-PCR
  - Flow cytometry analysis
  - Lesion measurements
  - Parasite load by quantitative real-time-PCR
- QUANTIFICATION AND STATISTICAL ANALYSIS
  - Statistical analysis

SUPPLEMENTAL INFORMATION

Supplemental Information can be found online at https://doi.org/10.1016/j.celrep.2020.108317.

ACKNOWLEDGMENTS

We thank Ana Beatriz F. Barletta (LMVR, National Institute of Allergy and Infectious Diseases [NIAID]), Owen M. Schwartz, and Margery Smelkinson (Biological Imaging Facility, Research Technology Branch, NIAID) for their support with the confocal microscope and Lucas Tirloni (LMVR, NIAID) for his insights into tick biology. The graphical abstract is courtesy of Visual Medical Arts, NIAID, Rocky Mountain Labs; the illustration is by Ryan Kissinger. This research was supported by the Intramural Research Program of the NIH, NIAID. The findings of this study are an informal communication and represent the FDA authors' own best judgments. These comments do not bind or obligate the Food and Drug Administration.

AUTHOR CONTRIBUTIONS

T.D.-V. and E.I. contributed equally to this study and carried out most of the experiments and data analysis. T.D.S., W.d.C., M.M.D., and P.C. assisted with sand fly infections and transmission experiments. T.D.S. assisted with confocal microscopy and image preparation and analysis; J.R.L., S. Karmakar, and R.D. performed RNA- and DNA-based experiments and related analyses. B.M.N. and I.N.M. optimized staining of slides for confocal imaging. S.C. and M.P.S. generated and provided *HMOX1*$^{lox/lox}$ and *HMOX1*$^{R26\Delta/\Delta}$ mice. C.M. and D.E.S. reared and provided arthropods throughout the study. V.M.B., H.L.N., M.P.S., F.O., and J.G.V. contributed to experimental design and data interpretation. S. Kamhawi, T.D.-V., and E.I. conceived the study, interpreted the data, and wrote the manuscript with intellectual input from J.G.V. and M.P.S. All authors read and commented on the paper.

DECLARATION OF INTERESTS

The authors declare no competing interests.

Received: April 24, 2020
Revised: September 3, 2020
Accepted: October 6, 2020
Published: October 27, 2020

REFERENCES

Alam, M.Z., Devalaraja, S., and Haldar, M. (2017). The heme connection: linking erythrocytes and macrophage biology. Front. Immunol. *8*, 33.

Atayde, V.D., Aslan, H., Townsend, S., Hassani, K., Kamhawi, S., and Olivier, M. (2015). Exosome secretion by the parasitic protozoan Leishmania within the sand fly midgut. Cell Rep. *13*, 957–967.

Belkaid, Y., Kamhawi, S., Modi, G., Valenzuela, J., Noben-Trauth, N., Rowton, E., Ribeiro, J., and Sacks, D.L. (1998). Development of a natural model of cutaneous leishmaniasis: powerful effects of vector saliva and saliva preexposure on the long-term outcome of Leishmania major infection in the mouse ear dermis. J. Exp. Med. *188*, 1941–1953.

Brifault, C., Gilder, A.S., Laudati, E., Banki, M., and Gonias, S.L. (2017). Shedding of membrane-associated LDL receptor-related protein-1 from microglia amplifies and sustains neuroinflammation. J. Biol. Chem. *292*, 18699–18712.

Brogliato, A.R., Moor, A.N., Kesl, S.L., Guilherme, R.F., Georgii, J.L., Peters-Golden, M., Canetti, C., Gould, L.J., and Benjamim, C.F. (2014). Critical role of 5-lipoxygenase and heme oxygenase-1 in wound healing. J. Invest. Dermatol. *134*, 1436–1445.

Buechler, C., Ritter, M., Orsó, E., Langmann, T., Klucken, J., and Schmitz, G. (2000). Regulation of scavenger receptor CD163 expression in human monocytes and macrophages by pro- and antiinflammatory stimuli. J. Leukoc. Biol. *67*, 97–103.

Calvo, E., Mans, B.J., Andersen, J.F., and Ribeiro, J.M. (2006). Function and evolution of a mosquito salivary protein family. J. Biol. Chem. *281*, 1935–1942.

Costa, D.L., Namasivayam, S., Amaral, E.P., Arora, K., Chao, A., Mittereder, L.R., Maiga, M., Boshoff, H.I., Barry, C.E., 3rd, Goulding, C.W., et al. (2016). Pharmacological inhibition of host heme oxygenase-1 suppresses Mycobacterium tuberculosis infection in vivo by a mechanism dependent on T lymphocytes. MBio *7*, e01675-16.

Devey, L., Ferenbach, D., Mohr, E., Sangster, K., Bellamy, C.O., Hughes, J., and Wigmore, S.J. (2009). Tissue-resident macrophages protect the liver from ischemia reperfusion injury via a heme oxygenase-1-dependent mechanism. Mol. Ther. *17*, 65–72.

Dey, R., Joshi, A.B., Oliveira, F., Pereira, L., Guimarães-Costa, A.B., Serafim, T.D., de Castro, W., Coutinho-Abreu, I.V., Bhattacharya, P., Townsend, S., et al. (2018). Gut microbes egested during bites of infected sand flies augment

severity of Leishmaniasis via inflammasome-derived IL-1β. Cell Host Microbe *23*, 134–143.e6.

Epelman, S., Lavine, K.J., Beaudin, A.E., Sojka, D.K., Carrero, J.A., Calderon, B., Brija, T., Gautier, E.L., Ivanov, S., Satpathy, A.T., et al. (2014). Embryonic and adult-derived resident cardiac macrophages are maintained through distinct mechanisms at steady state and during inflammation. Immunity *40*, 91–104.

Epiphanio, S., Mikolajczak, S.A., Gonçalves, L.A., Pamplona, A., Portugal, S., Albuquerque, S., Goldberg, M., Rebelo, S., Anderson, D.G., Akinc, A., et al. (2008). Heme oxygenase-1 is an anti-inflammatory host factor that promotes murine plasmodium liver infection. Cell Host Microbe *3*, 331–338.

Ferreira, A., Marguti, I., Bechmann, I., Jeney, V., Chora, A., Palha, N.R., Rebelo, S., Henri, A., Beuzard, Y., and Soares, M.P. (2011). Sickle hemoglobin confers tolerance to Plasmodium infection. Cell *145*, 398–409.

Franklinos, L.H.V., Jones, K.E., Redding, D.W., and Abubakar, I. (2019). The effect of global change on mosquito-borne disease. Lancet Infect. Dis. *19*, e302–e312.

Giraud, E., Lestinova, T., Derrick, T., Martin, O., Dillon, R.J., Volf, P., Műller, I., Bates, P.A., and Rogers, M.E. (2018). Leishmania proteophosphoglycans regurgitated from infected sand flies accelerate dermal wound repair and exacerbate leishmaniasis via insulin-like growth factor 1-dependent signalling. PLoS Pathog. *14*, e1006794.

Gozzelino, R., Jeney, V., and Soares, M.P. (2010). Mechanisms of cell protection by heme oxygenase-1. Annu. Rev. Pharmacol. Toxicol. *50*, 323–354.

Grochot-Przeczek, A., Lach, R., Mis, J., Skrzypek, K., Gozdecka, M., Sroczynska, P., Dubiel, M., Rutkowski, A., Kozakowska, M., Zagorska, A., et al. (2009). Heme oxygenase-1 accelerates cutaneous wound healing in mice. PLoS ONE *4*, e5803.

Hauptmann, J., Johann, L., Marini, F., Kitic, M., Colombo, E., Mufazalov, I.A., Krueger, M., Karram, K., Moos, S., Wanke, F., et al. (2020). Interleukin-1 promotes autoimmune neuroinflammation by suppressing endothelial heme oxygenase-1 at the blood-brain barrier. Acta Neuropathol. *140*, 549–567.

Keeney, S.E., Schmalstieg, F.C., Palkowetz, K.H., Rudloff, H.E., Le, B.M., and Goldman, A.S. (1993). Activated neutrophils and neutrophil activators in human milk: increased expression of CD11b and decreased expression of L-selectin. J. Leukoc. Biol. *54*, 97–104.

Larsen, R., Gozzelino, R., Jeney, V., Tokaji, L., Bozza, F.A., Japiassú, A.M., Bonaparte, D., Cavalcante, M.M., Chora, A., Ferreira, A., et al. (2010). A central role for free heme in the pathogenesis of severe sepsis. Sci. Transl. Med. *2*, 51ra71.

Lavoipierre, M.M. (1965). Feeding mechanism of blood-sucking arthropods. Nature *208*, 302–303.

Leid, J., Carrelha, J., Boukarabila, H., Epelman, S., Jacobsen, S.E., and Lavine, K.J. (2016). Primitive embryonic macrophages are required for coronary development and maturation. Circ. Res. *118*, 1498–1511.

Lerner, E.A., Ribeiro, J.M., Nelson, R.J., and Lerner, M.R. (1991). Isolation of maxadilan, a potent vasodilatory peptide from the salivary glands of the sand fly Lutzomyia longipalpis. J. Biol. Chem. *266*, 11234–11236.

Luz, N.F., Andrade, B.B., Feijó, D.F., Araújo-Santos, T., Carvalho, G.Q., Andrade, D., Abánades, D.R., Melo, E.V., Silva, A.M., Brodskyn, C.I., et al. (2012). Heme oxygenase-1 promotes the persistence of Leishmania chagasi infection. J. Immunol. *188*, 4460–4467.

Luz, N.F., DeSouza-Vieira, T., De Castro, W., Vivarini, A.C., Pereira, L., França, R.R., Silveira-Mattos, P.S., Costa, D.L., Teixeira, C., Meneses, C., et al. (2018). *Lutzomyia longipalpis* saliva induces heme oxygenase-1 expression at bite sites. Front. Immunol. *9*, 2779.

Martin, P. (1997). Wound healing–aiming for perfect skin regeneration. Science *276*, 75–81.

Martin-Martin, I., Paige, A., Valenzuela Leon, P.C., Gittis, A.G., Kern, O., Bonilla, B., Chagas, A.C., Ganesan, S., Smith, L.B., Garboczi, D.N., and Calvo, E. (2020). ADP binding by the Culex quinquefasciatus mosquito D7 salivary protein enhances blood feeding on mammals. Nat. Commun. *11*, 2911.

Martins, R., Carlos, A.R., Braza, F., Thompson, J.A., Bastos-Amador, P., Ramos, S., and Soares, M.P. (2019). Disease tolerance as an inherent component of immunity. Annu. Rev. Immunol. *37*, 405–437.

Mason, L.M., Veerman, C.C., Geijtenbeek, T.B., and Hovius, J.W. (2014). Ménage à trois: Borrelia, dendritic cells, and tick saliva interactions. Trends Parasitol. *30*, 95–103.

Medzhitov, R., Schneider, D.S., and Soares, M.P. (2012). Disease tolerance as a defense strategy. Science *335*, 936–941.

Motterlini, R., and Otterbein, L.E. (2010). The therapeutic potential of carbon monoxide. Nat. Rev. Drug Discov. *9*, 728–743.

Murray, T.S., Okegbe, C., Gao, Y., Kazmierczak, B.I., Motterlini, R., Dietrich, L.E., and Bruscia, E.M. (2012). The carbon monoxide releasing molecule CORM-2 attenuates Pseudomonas aeruginosa biofilm formation. PLoS One *7*, e35499.

Nairz, M., Theurl, I., Swirski, F.K., and Weiss, G. (2017). "Pumping iron"-how macrophages handle iron at the systemic, microenvironmental, and cellular levels. Pflugers Arch. *469*, 397–418.

Nilsson, A., Vesterlund, L., and Oldenborg, P.A. (2012). Macrophage expression of LRP1, a receptor for apoptotic cells and unopsonized erythrocytes, can be regulated by glucocorticoids. Biochem. Biophys. Res. Commun. *417*, 1304–1309.

Nurden, A.T. (2011). Platelets, inflammation and tissue regeneration. Thromb. Haemost. *105* (*Suppl 1*), S13–S33.

Oliver, J.D., Lynn, G.E., Burkhardt, N.Y., Price, L.D., Nelson, C.M., Kurtti, T.J., and Munderloh, U.G. (2016). Infection of immature Ixodes scapularis (Acari: Ixodidae) by membrane feeding. J. Med. Entomol. *53*, 409–415.

Opneja, A., Kapoor, S., and Stavrou, E.X. (2019). Contribution of platelets, the coagulation and fibrinolytic systems to cutaneous wound healing. Thromb. Res. *179*, 56–63.

Otterbein, L.E., Soares, M.P., Yamashita, K., and Bach, F.H. (2003). Heme oxygenase-1: unleashing the protective properties of heme. Trends Immunol. *24*, 449–455.

Pamplona, A., Ferreira, A., Balla, J., Jeney, V., Balla, G., Epiphanio, S., Chora, A., Rodrigues, C.D., Gregoire, I.P., Cunha-Rodrigues, M., et al. (2007). Heme oxygenase-1 and carbon monoxide suppress the pathogenesis of experimental cerebral malaria. Nat. Med. *13*, 703–710.

Park, S.Y., and Kim, I.S. (2017). Engulfment signals and the phagocytic machinery for apoptotic cell clearance. Exp. Mol. Med. *49*, e331.

Paudel, S., Baral, P., Ghimire, L., Bergeron, S., Jin, L., DeCorte, J.A., Le, J.T., Cai, S., and Jeyaseelan, S. (2019). CXCL1 regulates neutrophil homeostasis in pneumonia-derived sepsis caused by *Streptococcus pneumoniae* serotype 3. Blood *133*, 1335–1345.

Pingen, M., Schmid, M.A., Harris, E., and McKimmie, C.S. (2017). Mosquito biting modulates skin response to virus infection. Trends Parasitol. *33*, 645–657.

Prates, D.B., Santos, L.D., Miranda, J.C., Souza, A.P., Palma, M.S., Barral-Netto, M., and Barral, A. (2008). Changes in amounts of total salivary gland proteins of Lutzomyia longipallpis (Diptera: Psychodidae) according to age and diet. J. Med. Entomol. *45*, 409–413.

Protzer, U., Seyfried, S., Quasdorff, M., Sass, G., Svorcova, M., Webb, D., Bohne, F., Hösel, M., Schirmacher, P., and Tiegs, G. (2007). Antiviral activity and hepatoprotection by heme oxygenase-1 in hepatitis B virus infection. Gastroenterology *133*, 1156–1165.

Ramos, S., Carlos, A.R., Sundaram, B., Jeney, V., Ribeiro, A., Gozzelino, R., Bank, C., Gjini, E., Braza, F., Martins, R., et al. (2019). Renal control of disease tolerance to malaria. Proc. Natl. Acad. Sci. USA *116*, 5681–5686.

Ready, P.D. (2013). Biology of phlebotomine sand flies as vectors of disease agents. Annu. Rev. Entomol. *58*, 227–250.

Ribeiro, J.M. (1995). Blood-feeding arthropods: live syringes or invertebrate pharmacologists? Infect. Agents Dis. *4*, 143–152.

Ribeiro, J.M.C., Modi, G.B., and Tesh, R.B. (1989). Salivary apyrase activity of some Old-World phlebotomine sand flies. Insect Biochem. *19*, 409–412.

Rogers, M.E., and Bates, P.A. (2007). Leishmania manipulation of sand fly feeding behavior results in enhanced transmission. PLoS Pathog. *3*, e91.

Sacks, D.L., Hieny, S., and Sher, A. (1985). Identification of cell surface carbohydrate and antigenic changes between noninfective and infective developmental stages of Leishmania major promastigotes. J. Immunol. *135*, 564–569.

Saha, S., Basu, M., Guin, S., Gupta, P., Mitterstiller, A.M., Weiss, G., Jana, K., and Ukil, A. (2019). *Leishmania donovani* exploits macrophage heme oxygenase-1 to neutralize oxidative burst and TLR signaling-dependent host defense. J. Immunol. *202*, 827–840.

Schaer, C.A., Deuel, J.W., Bittermann, A.G., Rubio, I.G., Schoedon, G., Spahn, D.R., Wepf, R.A., Vallelian, F., and Schaer, D.J. (2013). Mechanisms of haptoglobin protection against hemoglobin peroxidation triggered endothelial damage. Cell Death Differ. *20*, 1569–1579.

Serafim, T.D., Coutinho-Abreu, I.V., Oliveira, F., Meneses, C., Kamhawi, S., and Valenzuela, J.G. (2018). Sequential blood meals promote Leishmania replication and reverse metacyclogenesis augmenting vector infectivity. Nat. Microbiol. *3*, 548–555.

Shaw, W.R., and Catteruccia, F. (2019). Vector biology meets disease control: using basic research to fight vector-borne diseases. Nat. Microbiol. *4*, 20–34.

Shi, C., and Pamer, E.G. (2011). Monocyte recruitment during infection and inflammation. Nat. Rev. Immunol. *11*, 762–774.

Silva, R.C.M.C., Travassos, L.H., Paiva, C.N., and Bozza, M.T. (2020). Heme oxygenase-1 in protozoan infections: A tale of resistance and disease tolerance. PLoS Pathog. *16*, e1008599.

Silva-Gomes, S., Appelberg, R., Larsen, R., Soares, M.P., and Gomes, M.S. (2013). Heme catabolism by heme oxygenase-1 confers host resistance to Mycobacterium infection. Infect. Immun. *81*, 2536–2545.

Simões, M.L., Caragata, E.P., and Dimopoulos, G. (2018). Diverse host and restriction factors regulate mosquito-pathogen interactions. Trends Parasitol. *34*, 603–616.

Singh, N., Ahmad, Z., Baid, N., and Kumar, A. (2018). Host heme oxygenase-1: Friend or foe in tackling pathogens? IUBMB Life *70*, 869–880.

Soares, M.P., and Hamza, I. (2016). Macrophages and iron metabolism. Immunity *44*, 492–504.

Sun, P., Nie, K., Zhu, Y., Liu, Y., Wu, P., Liu, Z., Du, S., Fan, H., Chen, C.H., Zhang, R., et al. (2020). A mosquito salivary protein promotes flavivirus transmission by activation of autophagy. Nat. Commun. *11*, 260.

Sutherland, T.E., Logan, N., Rückerl, D., Humbles, A.A., Allan, S.M., Papayannopoulos, V., Stockinger, B., Maizels, R.M., and Allen, J.E. (2014). Chitinase-like proteins promote IL-17-mediated neutrophilia in a tradeoff between nematode killing and host damage. Nat. Immunol. *15*, 1116–1125.

Svensjö, E., Saraiva, E.M., Bozza, M.T., Oliveira, S.M., Lerner, E.A., and Scharfstein, J. (2009). Salivary gland homogenates of Lutzomyia longipalpis and its vasodilatory peptide maxadilan cause plasma leakage via PAC1 receptor activation. J. Vasc. Res. *46*, 435–446.

Svensjö, E., Saraiva, E.M., Amendola, R.S., Barja-Fidalgo, C., Bozza, M.T., Lerner, E.A., Teixeira, M.M., and Scharfstein, J. (2012). Maxadilan, the Lutzomyia longipalpis vasodilator, drives plasma leakage via PAC1-CXCR1/2-pathway. Microvasc. Res. *83*, 185–193.

Szabo, I.L., Kenyeres, A., Szegedi, A., and Szollosi, A.G. (2018). Heme oxygenase and the skin in health and disease. Curr. Pharm. Des. *24*, 2303–2310.

Thomsen, J.H., Etzerodt, A., Svendsen, P., and Moestrup, S.K. (2013). The haptoglobin-CD163-heme oxygenase-1 pathway for hemoglobin scavenging. Oxid. Med. Cell. Longev. *2013*, 523652.

Titus, R.G., and Ribeiro, J.M. (1988). Salivary gland lysates from the sand fly Lutzomyia longipalpis enhance Leishmania infectivity. Science *239*, 1306–1308.

Vandivier, R.W., Ogden, C.A., Fadok, V.A., Hoffmann, P.R., Brown, K.K., Botto, M., Walport, M.J., Fisher, J.H., Henson, P.M., and Greene, K.E. (2002). Role of surfactant proteins A, D, and C1q in the clearance of apoptotic cells in vivo and in vitro: calreticulin and CD91 as a common collectin receptor complex. J. Immunol. *169*, 3978–3986.

Vanella, L., Barbagallo, I., Tibullo, D., Forte, S., Zappalà, A., and Li Volti, G. (2016). The non-canonical functions of the heme oxygenases. Oncotarget *7*, 69075–69086.

Yang, Q., Wang, Y., Pei, G., Deng, X., Jiang, H., Wu, J., Zhou, C., Guo, Y., Yao, Y., Zeng, R., and Xu, G. (2019). Bone marrow-derived Ly6C$^-$ macrophages promote ischemia-induced chronic kidney disease. Cell Death Dis. *10*, 291.

STAR★METHODS

KEY RESOURCES TABLE

REAGENT or RESOURCE	SOURCE	IDENTIFIER
Antibodies		
Rabbit anti-HO-1	abcam	Cat#ab13243; RRID: AB_299790
Rabbit anti-HSP90	Cell Signaling Technology	Cat#4877S; RRID: AB_2233307
Goat anti-rabbit secondary antibody conjugated to horseradish peroxidase	Cell Signaling Technology	Cat#7074S; RRID: AB_2099233
Goat anti-IBA-1	abcam	Cat#ab107159; RRID: AB_10972670
Rabbit anti-myeloperoxidase	abcam	Cat#ab9535; RRID: AB_307322
Rat anti-mouse TER-119 (clone TER-119)	BD Biosciences	Cat#550565; RRID: AB_393756
AF488 Donkey anti-rabbit	Thermo-Fisher Scientific	Cat#A-21206; RRID: AB_2535792
AF594 Donkey anti-mouse	Thermo-Fisher Scientific	Cat#A-21203; RRID: AB_141633
AF680 Donkey anti-goat	Thermo-Fisher Scientific	Cat#A-32860; RRID: AB_2762841
Biotinylated Donkey anti-rat	Novus Biologicals	Cat#NBP1-75379; RRID: AB_11027475
Streptavidin AF750	Thermo-Fisher Scientific	Cat#S21384; Temporary PRID: AB_2876869
TruStain FcX anti-mouse CD16/32 (clone 93)	Biolegend	Cat#101320; RRID: AB_1574975
PE-Cy7 anti-mouse/human CD11b (clone M1/70)	Biolegend	Cat#101216; RRID: AB_312799
FITC anti-mouse Ly6C (clone HK1.4)	Biolegend	Cat#128006; RRID: AB_1186135
PE anti-mouse Ly6G (clone 1A8)	Biolegend	Cat#127608; RRID: AB_1186099
PerCP anti-mouse F4/80 (clone BM8)	Biolegend	Cat#123126; RRID: AB_893483
PE anti-mouse CD163/M130 (clone TNKUPJ)	Bioss Antibodies	Cat#bs-2527R-PE; RRID: AB_11062797
PE anti-mouse CD91 (clone EPR3724)	abcam	Cat#ab225060; Temporary PRID: AB_2876868
APC anti-mouse IL1-β pro-form antibody (clone NJTEN3)	eBioscience	Cat#17-7114-80; RRID: AB_10670739
APC anti-mouse TER-119 (clone TER-119)	Biolegend	Cat#116212; RRID: AB_313713
Chemicals, Peptides, and Recombinant Proteins		
Low Phytoestrogen Rodent Diet	Teklad global-Envigo	Cat#2919
Liberase TL Research Grade	Roche	Cat#5401020001
Tin Protoporphyrin IX dichloride (SnPPIX)	Enzo Life Science	Cat#ALX-430-051-M025
Tricarbonyldichlororuthenium (II) dimer (CORM-2)	Sigma-Aldrich	Cat#288144
Pierce RIPA Lysis and Extraction Buffer	Thermo-Fisher Scientific	Cat#89901
Phenylmethylsulfonyl Fluoride solution	Sigma-Aldrich	Cat#93482
Halt Protease Inhibitor Cocktail	Thermo-Fisher Scientific	Cat#87786
Peanut Agglutinin (PNA), Unconjugated	Vector Laboratories	Cat#L-1070
Critical Commercial Assays		
Pierce BCA Protein Assay Kit	Thermo-Fisher Scientific	Cat#23227
Mouse Heme Oxygenase 1 ELISA Kit	abcam	Cat#ab204524
Mouse Hemoglobin ELISA Kit	abcam	Cat#ab157715
Flash Western Chemiluminescence	Azure Biosystems	Cat#AC221
PureLink RNA Mini kit	Invitrogen -Thermo-Fisher Scientific	Cat#12183020
cDNA reverse transcription kit	Applied Biosystems - Thermo-Fisher Scientific	Cat#4368813

(*Continued on next page*)

Continued

REAGENT or RESOURCE	SOURCE	IDENTIFIER
TaqMan gene expression master mix	Applied Biosystems - Thermo-Fisher Scientific	Cat#4369016
High Pure PCR Template Preparation Kit	Roche	Cat#11796828001
LIVE/DEAD Fixable Yellow Dead Cell Stain Kit	Thermo-Fisher Scientific	Cat#L34959
Fixation/Permeabilization Solution Kit	BD Biosciences	Cat#554714
Experimental Models: Cell Lines		
Leishmania major WR 2885 strain	LMVR/NIAID/NIH Originally isolated from a US soldier deployed to Iraq	N/A
Experimental Models: Organisms/Strains		
Mouse: C57BL/6	Charles River Laboratories	Strain Code #027
Mouse: C57BL/6 *R26*^{CreERT2} (B6.129-Gt (ROSA)26Sortm1 (cre/ERT2)Tyj/J)	The Jackson Laboratory	Cat#008463
Mouse: *Hmox1*$^{fl/fl}$	Instituto Gulbenkian de Ciência; (Ramos et al., 2019)	N/A
Mouse: R26$^{CreERT2/CreERT2}$Hmox$^{fl/fl}$ (*Hmox1*$^{R26fl/fl}$)	Instituto Gulbenkian de Ciência: (Ramos et al., 2019)	N/A
Mouse: C57BL/6 *Hmox1*$^{R26\Delta/\Delta}$	Instituto Gulbenkian de Ciência; (Ramos et al., 2019)	N/A
Mouse: Hmox1$^{lox/lox}$	Instituto Gulbenkian de Ciência; (Ramos et al., 2019)	N/A
Lutzomyia longipalpis (Jacobina colony)	LMVR/NIAID/NIH	N/A
Phebotomus duboscqi (Mali colony)	LMVR/NIAID/NIH	N/A
Aedes aegypti (Liverpool strain)	LMVR/NIAID/NIH	N/A
Anopheles gambie (G3 strain)	LMVR/NIAID/NIH	N/A
Ornithodorus turicata (Florida strain)	LMVR/NIAID/NIH	N/A
Oligonucleotides		
Leishmania forward primer JW11 (5′-CCTATT TTACACCAA CCCCCAGT-3′)	(Dey et al., 2018)	N/A
Leishmania reverse primer JW12 (5′-GGGTAGGGGCGT TCTGCGAAA-3′)	(Dey et al., 2018)	N/A
Leishmania TaqMan probe (5′- [Aminoc6+TxRed] RA AARKKVRTRCAGAAAYCC CGT [BHQ2]-3′)	(Dey et al., 2018)	N/A
Software and Algorithms		
FlowJo 10 Software	FlowJO, LLC	https://www.flowjo.com/solutions/flowjo/downloads
ImageJ.exe 1.52a Software	NIH	https://imagej.nih.gov/ij/download.html
Prism 8 Software	GraphPad Prism	https://www.graphpad.com/scientific-software/prism/
Imaris x64 9.5.0 Software	Oxford Instruments	https://imaris.oxinst.com/microscopy-imaging-software-free-trial
EndNote X9 Software	Web of Science Group	https://endnote.com/downloads/
Other		
Schneider's Drosophila Medium	GIBCO	Cat#21720001
Heat Inactivated Fetal Bovine Serum	GIBCO	Cat#16140-071
Penicillin/Streptomycin	GIBCO	Cat#15140122
Rabbit defibrinated blood	Spring Valley Laboratories	N/A

(*Continued on next page*)

Continued

REAGENT or RESOURCE	SOURCE	IDENTIFIER
iBlot 2 Transfer Stack 0.45 μm nitrocellulose membrane	Thermo-Fisher Scientific	Cat#IB23001
NuPAGE 4-12% Bis-Tris protein precast gels	Thermo-Fisher Scientific	Cat#NP0335BOX
NuPAGE LDS Sample Buffer (4X)	Thermo-Fisher Scientific	Cat#NP0007
NuPAGE Sample Reducing Agent (10X)	Thermo-Fisher Scientific	Cat#NP0009
NuPAGE MES SDS Running Buffer (20X)	Thermo-Fisher Scientific	Cat#NP0002
BOND Dewax Solution	Leica	Cat#DEWAX-SOLUTION
BOND Epitope Retrieval Solution 2	Leica	Cat#EPITOPE-RETRIEVAL-SOLUTION-2
Normal Donkey Serum	Jackson ImmunoResearch	Cat#017-000-121
Streptavidin Blocking Solution	Vector Laboratories	Cat#SP-2002
Biotin Blocking Solution	Vector Laboratories	Cat#SP-2001
M.O.M.® (Mouse on Mouse) Immunodetection Kit, Basic	Vector Laboratories	Cat#BMK-2202
Mouse Fc-Receptor Blocking Reagent	Miltenyi Biotec	Cat#130-092-575
Protein Blocker	Agilent Dako	Cat#X0909
ProLong Gold Antifade Mountang	Invitrogen	Cat#P36930
DAPI	Thermo-Fisher Scientific	Cat#62248
Medicon 50 μm	BD Biosciences	Cat#340591
Filcon 50 μm	BD Biosciences	Cat#340602
Cell Staining Buffer	Biolegend	Cat#420201
ACK Lysing solution Buffer	GIBCO	Cat#A10492-01

RESOURCE AVAILABILITY

Lead contact

Further information and requests regarding resources and reagents should be directed to and will be fulfilled by the Lead Contact, Shaden Kamhawi (skamhawi@niaid.nih.gov).

Materials availability

This study did not generate new unique reagents or mouse lines.

Data and code availability

This study did not generate any unique datasets or code. No custom code was used to analyze these data and all methods used are cited in the STAR Methods section. Original source data for figures in the paper is available (https://data.mendeley.com/datasets/b6kj7rj6vb/draft?a=c8c9a806-d7f2-408f-8008-6e9ad3da780b).

EXPERIMENTAL MODEL AND SUBJECT DETAILS

Mice

Female wild-type C57BL/6 mice (6-8 weeks old) were purchased from Charles River Laboratories and maintained under pathogen-free conditions at the NIAID Twinbrook animal facility in Rockville, MD. C57BL/6 *HMOX1R26*$\Delta^{/}\Delta$ and *HMOX1*$^{lox/lox}$ were kindly provided by Dr. Miguel P. Soares (Instituto Gulbenkian de Ciência, Oeiras, Portugal). C57BL/6 *R26*^{CreERT2} mice were obtained from the Jackson Laboratory (B6.129-*Gt (ROSA)26Sortm1 (cre/ERT2)Tyj*/J, #008463). Briefly, *R26*^{CreERT2} mice were crossed to *HMOX1*$^{flox/flox}$. The R26 locus allows for the expression of CreERT2 ubiquitously. The CreERT2 consists of mutated estrogen receptor (ERT2) fused to the Cre recombinase. The chimeric protein is inactive, but can be activated by Tamoxifen, which binds to ERT2 and promotes the nuclear translocation of Cre-ERT2, allowing for excision of target gene, here the *HMOX1*$^{flox/flox}$. Conditional gene deletion (*HMOX1R26*$\Delta^{/}\Delta$) was achieved in 4-5 weeks old mice, fed *ad libitum* with Low Phytoestrogen Diet (Teklad Global-Envigo; #2919) for 2 weeks followed by administration of Tamoxifen (Sigma-Aldrich) suspended in sterile corn oil (Sigma) (gavage, 4.5mg per mouse, 1x every second day, 10x). Alternatively, Tamoxifen was provided by *ad libitum* intake of Rat/Mouse diet with Tamoxifen (M-Z, Low phytoestrogen; 360 mg/kg TAM Citrate + Sucrose flavour, 10mm Soybean free diet, sterilized 25 kGy; Ssniff Spezialdiäten GmbH) for 4 weeks. *HMOX1* deletion was assessed by qRT-PCR in whole blood and *HMOX1R26*$\Delta^{/}\Delta$ mice were shipped to NIAID 8 weeks after

the last Tamoxifen gavage or 6 weeks after removal of Tamoxifen enriched diet. Control *HMOX1* $^{flox/flox}$ mice were treated with the same protocol (Figure S3B; Ramos et al., 2019). Studies were conducted with female mice with the exception of *HMOX1* conditional deletion experiment where male and female were used due to availability and randomly assigned to experimental groups. All animal experiments were approved by NIAID Animal Care and Use Committee under animal protocol LMVR4E. The NIAID DIR Animal Care and Use Program complies with the Guide for the Care and Use of Laboratory Animals and with the NIH Office of Animal Care and Use and Animal Research Advisory Committee guidelines.

Parasites

L. major (WR 2885) parasites originally isolated from a US soldier deployed to Iraq were maintained by serial passage in BALB/c mice. Parasites were grown in Schneider's medium (GIBCO) supplemented with 20% inactivated fetal bovine serum (GIBCO), 100U/mL penicillin, and 100 μL/mL streptomycin (GIBCO), and *L. major* metacyclic promastigotes were purified from stationary cultures (day 4-5) by negative selection of noninfective forms by incubating parasites with 20 μL of 2 mg/mL of peanut agglutinin (Vector Laboratories) for 15 min at room temperature as described (Sacks et al., 1985).

Sand flies, mosquitoes, and ticks rearing

Lutzomyia longipalpis (Jacobina colony) and *Phebotomus duboscqi* (Mali colony) were reared using as larval food a mixture of fermented rabbit feces and rabbit food. Adult sand flies were offered a cotton swab containing 30% sucrose prior and post-infection and maintained at 26°C with 75% humidity with 12-h light/dark cycle until use. *Aedes aegypti* (Liverpool strain) mosquitoes and *Anopheles gambiae* (G3 strain) were maintained at 28°C, 80% humidity, with a 12-h light/dark cycle and were provided a 10% Karo syrup solution. *Ornithodoros turicata* ticks were originally obtained from Old Dominion University (ODU). Nymphal ticks were allowed to feed in an artificial feeding set-up previously described (Oliver et al., 2016). After reaching the adult stage, ticks were kept in aerated 50mL conical tubes containing wood chip mulch at 26°C with 75% humidity with 12-h light/dark cycle until use. All vectors were reared and maintained at the Insectary Unit of Laboratory of Malaria and Vector Research, NIAID, NIH,

METHOD DETAILS

Sand fly infection

Four to six days old female *P. duboscqi* sand flies were artificially fed through a chicken skin membrane filled with rabbit defibrinated blood (Spring Valley Laboratories) spiked with 1-2x10^6 *L. major* amastigotes/mL. After 2h, blood fed flies were separated and maintained at 26°C with 75% humidity until they developed a mature infection (1BM) with >75% metacyclic promastigotes, which was assessed by Phase-contrast microscopy of dissect midguts. Infected sand flies generally reached a mature infection by 12-20 days. For experiments undertaken to assess cutaneous leishmaniasis pathology, infected sand flies were subjected to a second uninfected blood meal (2BM) by feeding on Swiss mice to generate a more homogeneous infection, and a mixture of 1BM and 2BM flies were used to maximize transmission success (Serafim et al., 2018). At day 11 to 19 post-infection, sand fly midguts (n = 8-11) were dissected and the number of parasites and percentage of metacyclic promastigotes per midgut were determined prior to transmission.

Salivary gland homogenate

Salivary glands from *Phlebotomus duboscqi* (Mali colony) and *Lutzomyia longipalpis* (Jacobina colony) sand flies, *Anopheles gambie* (G3 strain) and *Aedes aegypti* (Liverpool strain) mosquitoes, and *Ornithodoros turicata* ticks (Florida strain) were dissected and sonicated for three cycles followed by centrifugation at 10,000xg for 3 min at 4°C. Supernatant was then collected and used for experiments.

Mice exposure to vector bites or needle pokes

Mice were anesthetized by i.p. injection of a mixture of ketamine (100mg/kg) and xylazine (10mg/kg). For cutaneous leishmaniasis pathology experiments, mice ears were exposed to 10 infected sand flies combining 1BM and 2BM flies (30%–50%) for 2 h in the dark. Animals were kept for an extra hour when sand fly feeding could not be detected on randomly selected ears. For the remaining experiments, mouse ears were exposed to 5-20 uninfected sand flies, 10 *Aedes aegypti* or *Anopheles gambiae*, or 3 soft ticks (*Ornithodorus turicata*) for 1h, in the dark. Midpoint of each exposure period was used to calculate time points after bites. The number of fully blood-fed insects per mouse ear was determined for each experiment. To simulate mechanical damaged by vector probing, mice ears were randomly poked at the mouse ear 10 times with a 32-gauge needle.

Immunoblotting and ELISA immunosorbent assays

Mice ears were harvested, split into dorsal and ventral halves, and placed in RIPA lysis buffer (Thermo-Fisher Scientific) supplemented with phenylmethylsulfonyl fluoride (PMSF) (Sigma-Aldrich) and Halt Protease Inhibitor Cocktail (Thermo-Fisher Scientific). Next, mice ears were submitted to mechanical disruption using the Medimachine system (BD Biosciences). The soluble fraction of the lysate was recovered after centrifugation. Protein concentration was determined by the Pierce BCA Protein Assay Kit (Thermo-Fisher Scientific). For immunoblotting, proteins (20-40 μg) were denaturated in NuPAGE LDS Sample Buffer (Thermo-Fisher

Scientific) supplemented with NuPAGE Sample Reducing Agent with DL-Dithiothreitol (DTT) (Thermo-Fisher Scientific) under 95°C for 5 min. Then, proteins were separated by electrophoresis using NuPAGE 4%–12% Bis-Tris protein precast gels (Thermo-Fisher Scientific) and transferred to an iBlot 2 Transfer Stack 0.45 μm nitrocellulose membrane using the iBlot 2 Gel Transfer Device (Thermo-Fisher Scientific). Membranes were blocked overnight at 4°C with Tris-Buffered Saline, 0.1% TWEEN 20 (TBST) in 5% non-fat dry milk followed by the addition of rabbit anti-HO-1 antibody (abcam, Cat No. ab13243) or rabbit anti-HSP90 (Cell Signaling Technology, Cat No. 4877S) at a 1:500 dilution. Membranes were washed three times with TBST followed by 30 min incubation with Goat anti-rabbit secondary antibody conjugated to horseradish peroxidase (HRP) (Cell Signaling Technology, Cat No. 70745) at 1:10000. Each blot was developed by the addition of Flash Western Chemiluminescence Kit (Azure Biosystems) and the signal was captured after 2 min with Azure c600 chemiluminescence imager (Azure Biosystems). For densitometry, HO-1 and truncated HO-1 band densities were normalized against HSP90 band density on ImageJ 1.52a. Data were presented as fold change over naive for experimental samples. For enzyme-linked immunosorbent assay (ELISA), HO-1 and hemoglobin levels from ear skin tissue lysates were diluted at 1:20 and 1:10000, respectively. Quantification of proteins was performed using a Mouse HO-1 ELISA Set (abcam) and Hemoglobin Mouse ELISA Kit (abcam) according to the manufacturer's instructions.

Immunohistochemistry and confocal microscopy

Mouse ears exposed to infected or uninfected *P. duboscqi* sand flies bites were fixed with 10% buffered formalin phosphate solution and paraffin embedded as previously described (Dey et al., 2018). Slides were stained with Hematoxylin and eosin (H&E) and images were captured in REVOLVE4 Upright (Echo Laboratories) and acquired by an BF 12mp CMOS camera. Immunofluorescence (IF) of paraffin embedded skin sections was performed on the Leica Bond-RX automated system. Tissue sections were heated to 72°C for 30 min in Bond Dewax Solution (Leica) and rehydrated with absolute alcohol washes and 1 × ImmunoWash (StatLab). Bond Epitope Retrieval Solution 2 (Leica) was applied to sections and heated to 100°C for 20 min for Heat-Induced Epitope Retrieval (HIER). Tissues were blocked for 15 min each with 5% Normal Donkey Serum (Jackson ImmunoResearch), Streptavidin Blocking Solution (Vector Laboratories) and Biotin Blocking Solution (Vector Laboratories). Tissues were then blocked with Mouse on Mouse IgG Blocking Reagent (Vector Laboratories) for 60 min, 1:100 Mouse Fc-Receptor Blocking Reagent (Miltenyi Biotec) for 10 min, and Protein Blocker (Dako) for 30 min. Thereafter, tissues were incubated with the following primary antibodies: IBA-1 (polyclonal, abcam, Cat No. ab107159), HO-1 (polyclonal, abcam, Cat No. ab13243), myeloperoxidase (polyclonal, abcam, Cat No. ab9535), TER-119 (clone: TER-119, BD biosciences, Cat No. 550565) antibodies, and stained with DAPI (Thermo-Fisher Scientific). Samples were rinsed with ImmunoWash prior to a 30 min incubation in a cocktail mixture of donkey (Dk) host secondary antibodies. The secondary antibodies include AF488 Dk anti-rabbit (Thermo-Fisher Scientific, Cat No. A-21206), AF594 Dk anti-mouse (Thermo-Fisher Scientific, Cat No. A-21203), AF680 Dk anti-goat (Thermo-Fisher Scientific, Cat No. A-32860) and Biotinylated Dk anti-rat (Novus Biologicals, Cat No. 75379). Tissues were further incubated in Streptavidin AF750 (Thermo-Fisher Scientific, Cat No. S21384) for 30 min. Slides were counterstained with DAPI (Thermo-Fisher Scientific) at 1 μg/mL in 1x PBS for 2 min prior to mounting in ProLong Gold Antifade Mounting media (Invitrogen). Images were acquired by Leica TCS SP8 X and analyzed on Imaris x64 9.5.0 software. Images contrast was adjusted using a display adjustment window and a Gaussian filter was applied to each channel. Areas where macrophages were erythrophagocytosing RBCs were selected on a plane view. Using the Orhtogonal Slicer tool we compiled the Z stacks of selected areas (1-3) to show a transversal view through the cell adjusted on the slice orientation setting to XZ or YZ orthogonal view as indicated.

SnPPIX and CORM-2 treatment

Tin Protoporphyrin IX dichloride (SnPPIX) from Enzo Life Sciences was diluted as described (Costa et al., 2016). Briefly, SnPPIX was initially dissolved in PBS solution and full solubility was achieved by gradually adding droplets of NaOH 0.1M solution; pH was adjusted to 7-7.4 and stocked as 10mg/mL at −80°C until use. Wild-type female C57BL/6 mice were treated i.p. with 5mg/kg/mouse of SnPPIX or PBS the day before, the day of, and the day after vector-transmission. Tricarbonyldichlororuthenium (II) dimer (CORM-2) purchased from Sigma-Aldrich was diluted as previously described (Murray et al., 2012). Briefly, CORM-2 was diluted in PBS containing DMSO (10mM), aliquots of 25mg/mL were kept on −80°C. Solution was further diluted prior to use and CORM-2 (1mg/kg/mouse ear) or vehicle were administrated i.d. in the ear 2h after vector-transmission and ears were collected 6h after transmission.

Cytokine determination by quantitative RT-PCR

Cytokine expression in mice ears were determined by quantitative RT-PCR at 18h and 24h after vector-transmission. Briefly, total RNA from individual mice ears were extracted using PureLink RNA Mini kit (Invitrogen™ – Thermo-Fisher Scientific). Aliquots (300ng) of total RNA were reverse transcribed into cDNA using random hexamers from a high-capacity cDNA reverse transcription kit (Applied Biosystems). The cDNA was amplified with the TaqMan gene expression master mix (Applied Biosystems) and gene specific primer sets for *IL1B*, *IL10*, *CXCL1*, *CCL2*, *CHI3L1*, *NFE2L2*, *SLC40A1*, *HMOX1*, *NOS2*, *PTGS2* and *SOD1* using a CFX96 Touch Real-Time System (BioRad). Data were analyzed with CFX Manager Software. The gene expression levels were determined by the 2-ΔΔCt method; samples were normalized to *GAPDH* RNA expression and the results are expressed relative to expression values from naive mice. TaqMan Gene expression Assay ID: *IL1B* Mm00434228_m1; *IL10* Mm00439614_m1; *CCL2* Mm00441242_m1; *CXCL1* Mm04207460_m1; *CHI3L1* Mm00657889_mH; *NFE2L2* Mm00477784_m1; *SLC40A1* Mm01254822_m1; *HMOX1*

Mm00516005_m1; *NOS2* Mm00440502_m1; *SOD1* Mm01344233_g1; *PTGS2* Mm03294838_g1; *GAPDH* Mm99999915_g1 (Thermo-Fisher Scientific). Further details are provided in Table S1.

Flow cytometry analysis

Mouse ears were collected and placed in 1mL of PBS, then dorsal and ventral halves were separated and incubated in PBS containing Liberase TL (Roche) for 1h at 37°C and 5% CO_2. After digestion, ear sheets were placed in a Medicon (BD biosciences) and processed by mechanical disruption using the Medimachine tissue homogenizer system (BD biosciences). Cells were filtered in a 70 μm filcon (BD biosciences), and single cell suspensions were stained with anti-mouse CD16/32 (TruStain FcX, clone 93; Biolegend, Cat No. 101320) and CD11b (clone: M1/70, Cat No. 101216), LY6C (clone:HK1.4, Biolegend, Cat No.128006), Ly6G (clone: 1A8, Biolegend, Cat No. 127608), F4/80 (clone: BM8, Biolegend, Cat No. 123126), CD163/M130 (clone: TNKUPJ, Bioss, Cat No. bs-2527R) and CD91 (clone: EPR3724, abcam, Cat No. ab225060) for 30 min. The cells were then fixed and permeabilized with BD Cytofix/Cytoperm (BD Bioscience) followed by incubation of IL1-β pro-form (clone: NJTEN3; eBioscience, Cat No. 17-7114-80), or TER-119 (clone: TER-119, Biolegend, Cat No. 116212), for an additional 30 min. Of note, extracellular red blood cells were lysed with ACK solution (Sigma-Aldrich) for 60 s and prior to surface and intracellular staining with TER-119. Dead cells were excluded by staining with LIVE/DEAD fixable yellow dead cell stain kit (Thermo-Fisher Scientific). Cells were acquired on MACSQuant flow cytometer (Miltenyi Biotec) and data were analyzed with FlowJo 10 Software.

Lesion measurements

Weekly lesion measurements of mice exposed to infected sand fly bites were recorded using a digital caliper and the sum of all lesions diameter (mm) per ear were graphed.

Parasite load by quantitative real-time-PCR

A single cell suspension from mouse ears was used to establish parasite load quantification by qPCR as previously described (Dey et al., 2018). Briefly, DNA was extracted from 200 μL of cell suspension following the manufacturer's instructions from High pure PCR Template Preparation Kit (Roche Diagnostics) and a total of 75ng of DNA was used as template. Amplification of kinetoplast minicircle DNA of *Leishmania* was achieved using primers JW11 (5′-CCTATT TTACACCAA CCCCCAGT-3′), JW12 (5′-GGGTAGGG GCGTTCTGCGAAA-3′), and TaqMan probe (5′- [Aminoc6+TxRed] RAAARKKVRTRCAGAAAYCCCGT [BHQ2]-3′) (Dey et al., 2018). A standard curve was produced by spiking naive mice ears with a known number of *L. major* metacyclic promastigotes purified from sand fly midguts (Figure S3C). Standard curve was obtained by linear regression analysis of cycle threshold (Ct) values versus known number of *L. major* parasites ($\log^{10}$), and the slope, equation of the line, and R^2 values were calculated. The number of parasites from experimental samples was determined by fitting the cycle threshold (Ct) values in the equation of the line. All samples were run in duplicate in CFX96 Touch Real-Time PCR Detection System, Bio-Rad.

QUANTIFICATION AND STATISTICAL ANALYSIS

Statistical analysis

Data were analyzed and graphed using GraphPad Prism 8.0 software. Graphs represent the mean ± SEM or the median for Figure S2. Data are representative of multiple independent experiments, unless otherwise specified in their figure legend. Further statistical details of each experiment can be found at their respective figure legends. Kruskall Wallis with Dunn's post hoc analysis, or Mann–Whitney *U*-test statistical tests were performed using GraphPad Prism 8.0 software. *$p \leq 0.05$, **$p \leq 0.01$, ***$p \leq 0.001$, ****$p \leq 0.0001$ were considered significant.

Cell Reports, Volume *33*

Supplemental Information

Heme Oxygenase-1 Induction by Blood-Feeding Arthropods Controls Skin Inflammation and Promotes Disease Tolerance

Thiago DeSouza-Vieira, Eva Iniguez, Tiago D. Serafim, Waldionê de Castro, Subir Karmakar, Maria M. Disotuar, Pedro Cecilio, Joshua R. Lacsina, Claudio Meneses, Bianca M. Nagata, Silvia Cardoso, Daniel E. Sonenshine, Ian N. Moore, Valeria M. Borges, Ranadhir Dey, Miguel P. Soares, Hira L. Nakhasi, Fabiano Oliveira, Jesus G. Valenzuela, and Shaden Kamhawi

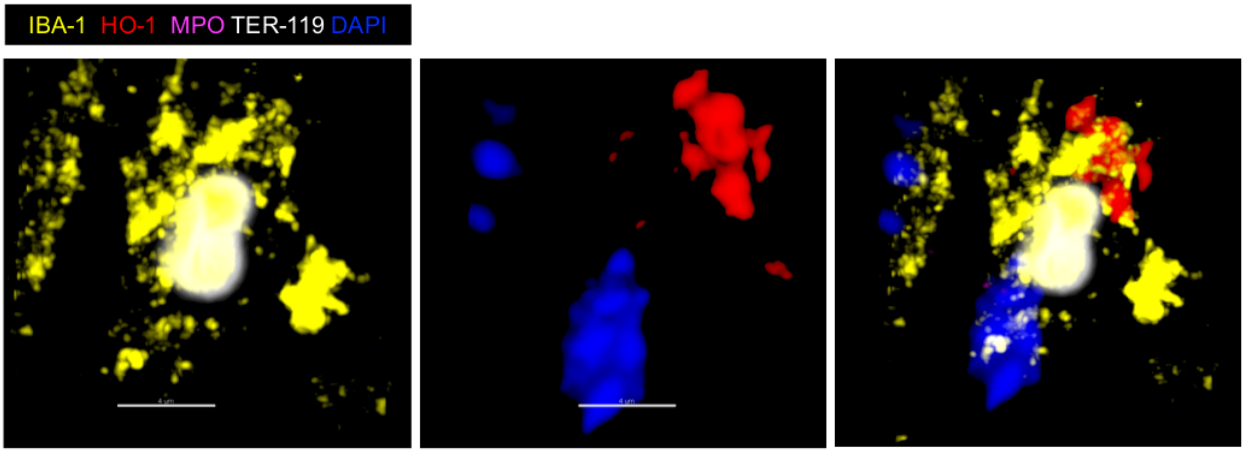

Figure S1. A tridimensional view of erythrophagocytosis. Related to Figure 2. Mouse ears were exposed to 20 *P. duboscqi* sand flies. Mice ears were collected at 18h after vector bites. Paraffin embedded skin sections were immunolabeled with IBA-1 (macrophages), HO-1 (HO-1), myeloperoxidase (MPO, neutrophils), TER-119 (RBCs) antibodies, stained for DAPI (nuclei) and visualized by confocal microscopy. Images are representative of 2 independent experiments (n = 4 mice ears/experiment).

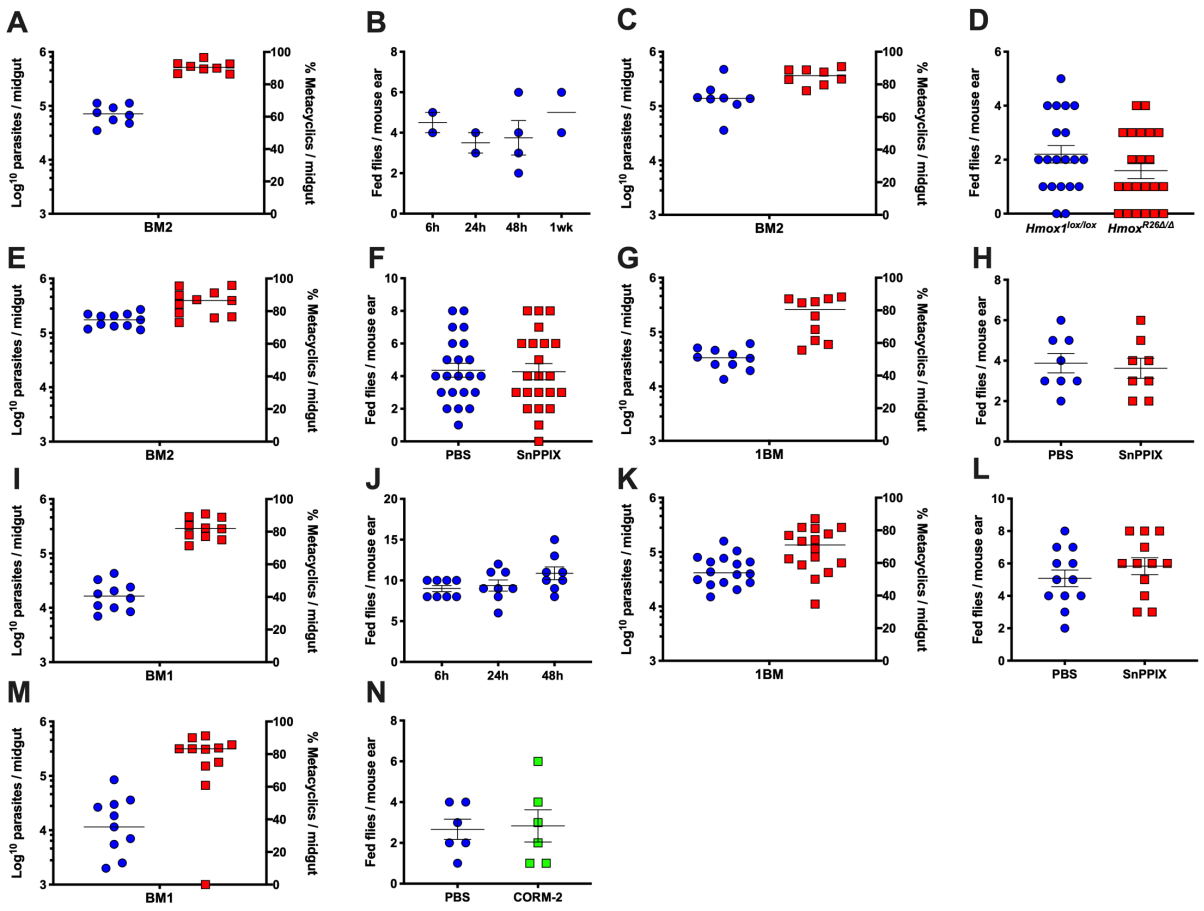

Figure S2. Infection status and feeding score of *L. major*-infected *P. duboscqi* sand flies used for transmission. Related to Figure 3 and 4. (A and B) Related to Figure 3, (A and B). (A) Infection status. (B) Feeding score after 6h, 24h, 48h, or 1wk post-transmission. (C and D) Related to Figure 3, (C) and (E and F). (C) Infection status. (D) Feeding score after transmission to *Hmox1*$^{lox/lox}$ or *Hmox1*$^{R26\Delta/\Delta}$ mice. (E and F) Related to Figure 3, (H and I). (E) Infection status. (F) Feeding score after transmission to SnPPIX- or PBS-treated mice. (G and H) Related to Figure 3, (J and K). (G) Infection status. (H) Feeding score after transmission to SnPPIX- or PBS-treated mice. (I and J) Related to Figure 4, (A and B). (I) Infection status. (J) Feeding score after 6h, 24h or 48h post-transmission. (K and L) Related to Figure 4, (C-E). (K) Infection status. (L) Feeding score after transmission to SnPPIX- or PBS-treated mice. (M and N) Related to Figure 4, (G and H). (M) Infection status. (N) Feeding score after transmission to CORM-2- or PBS-treated mice. Infection status, the number of parasites and percentage of metacyclics per midgut that received an infected blood meal (1BM) followed by a second uninfected blood meal (2BM). Feeding score, the number of fed infected sand flies per mouse ear. Graphs represent median (A), (C), (E), (G), (I), (K), (M) or mean ± SEM (B), (D), (F), (H), (J), (L), (N) of a representative data set from 2 (A), (B), (C), (D), (E), (F), (G), (H), (I), (J), or 3 (K), (L), or 5 (M), (N) independent experiments. *$P \leq 0.05$; Mann–Whitney *U*-test (D), (F), (H), (L), (N) and Kruskall Wallis with Dunn's *post hoc* analysis (B), (J).

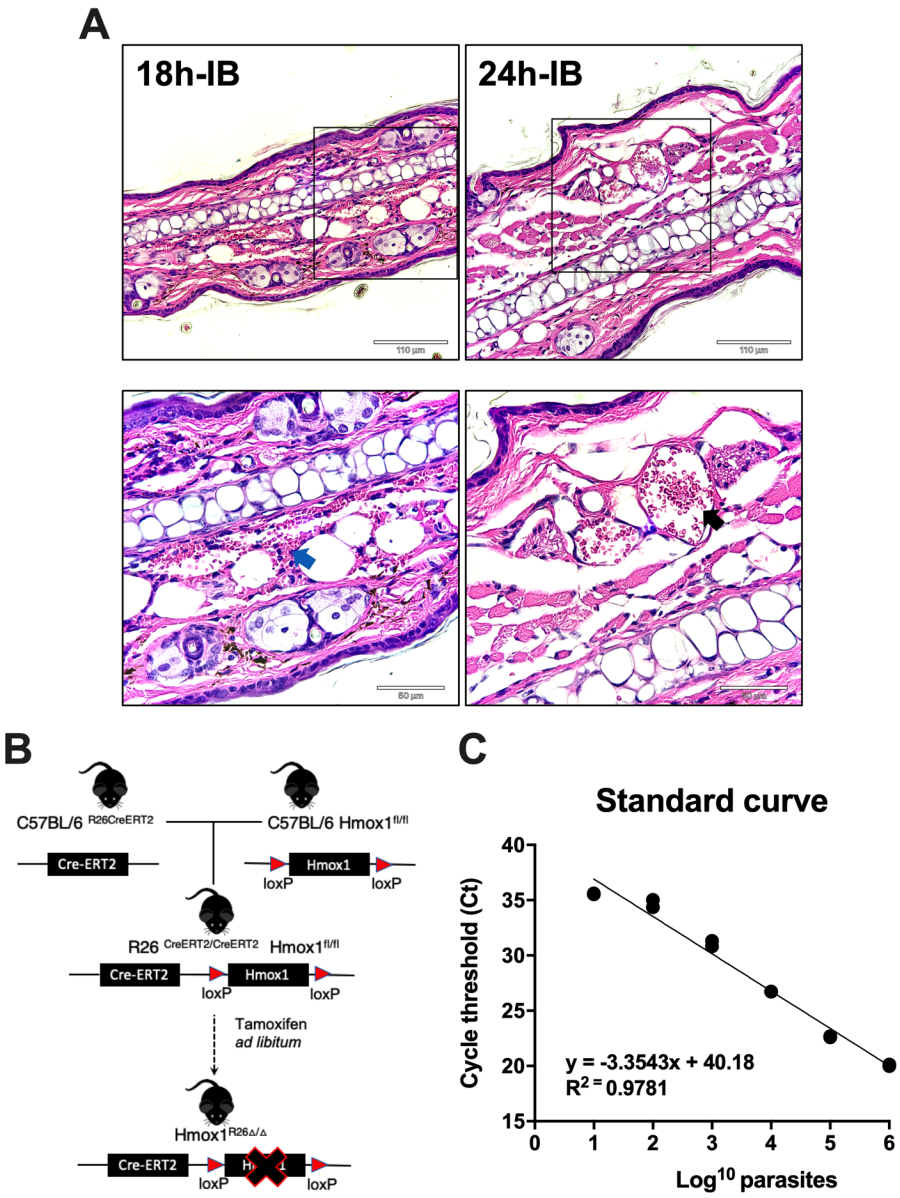

Figure S3. HO-1 induction after *Leishmania*-infected sand fly challenge. Related to Figure 3. (A) Histological analysis of host skin sections from sites exposed to infected sand fly bites. H&E skin sections representative of an ear from mice 18h or 24h after exposure to bites of 20 *L. major*-infected *P. duboscqi* sand flies. The selected area is magnified to highlight leakage of RBCs from vessels into the surrounding tissue (blue arrow). The black arrow points to RBCs inside a vessel at steady state. Scale bar, 110µm or 50µm. Images are representative of 2 independent experiments (n = 4 mice ears/experiment). (B) Generation of conditional knockout mice Hmox1R26Δ/Δ for challenge by infected bites. Crossing of $R26^{Cre\text{-}ERT2}$ and $Hmox1^{flox/flox}$ mice results in a transgene ($R26^{CreERT2/CreERT2}$ $Hmox1^{fl/fl}$) expressing *Hmox1* flanked by *loxP* regions and a mutated estrogen receptor fused to Cre recombinase (Cre-ERT2). Cre-ER only becomes activated upon tamoxifen binding, leading to its nuclear translocation and recombination of *Hmox1*. (C) Quantification of parasite burden by real time-PCR after challenge with infected sand flies. Representative standard curve produced by purification of DNA from naïve mice ears spiked with a known number of *L. major* metacyclic promastigotes purified from culture. Graph shows duplicates for each sample dilution from 1 of 2 experiments.

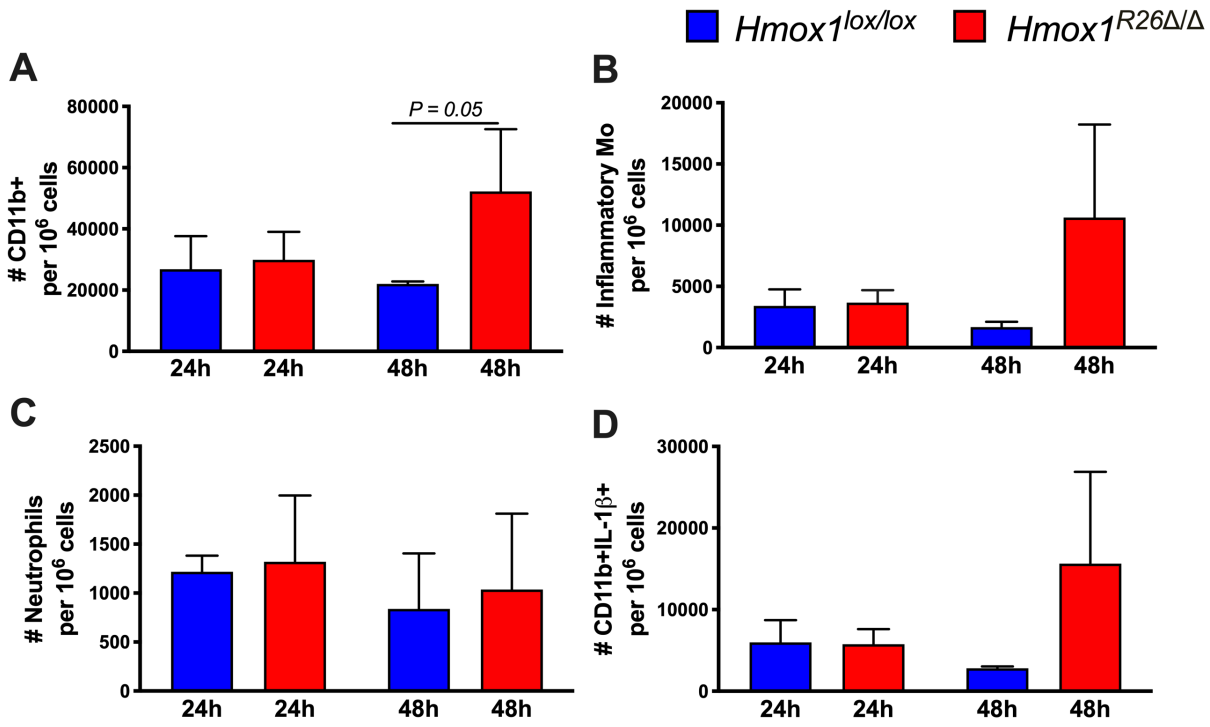

Figure S4. Deletion of HO-1 increases leukocyte infiltration and inflammation after infected sand fly bites. Related to Figure 4. (A-D) Ears of Hmox1lox/lox, Hmox1R26Δ/Δ or naïve mice were exposed to 20 L. major-infected P. duboscqi bites. Single cell suspensions were obtained 24h and 48h after vector-transmission, stained and analyzed by FACS. The number of CD11b+ cells (A), inflammatory monocytes (B), neutrophils (C), and CD11b+ cells expressing IL-1β (D). Graphs represent mean ± SEM of cumulative data from 2-4 pooled ears per replicate with 1-3 replicates from 2 independent experiments (A-D). *P ≤ 0.05; Mann–Whitney U-test (A-D).

Table S1. List of target genes for quantitative RT-PCR analyzed from RNA extracted from mice ears 18h and 24h after vector-transmission. Related to Figure 3.

Target Gene	SOURCE	IDENTIFIER
TaqMan Gene expression *IL-1β* Assay	Thermo-Fisher Scientific	Cat#Mm00434228_m1
TaqMan Gene expression *IL-10* Assay	Thermo-Fisher Scientific	Cat#Mm00439614_m1
TaqMan Gene expression *CCL2* Assay	Thermo-Fisher Scientific	Cat#Mm00441242_m1
TaqMan Gene expression *CXCL1* Assay	Thermo-Fisher Scientific	Cat#Mm04207460_m1
TaqMan Gene expression *Chil3* Assay	Thermo-Fisher Scientific	Cat#Mm00657889_mH
TaqMan Gene expression *Nfe212* Assay	Thermo-Fisher Scientific	Cat#Mm00477784_m1
TaqMan Gene expression *Slc40a1* Assay	Thermo-Fisher Scientific	Cat#Mm01254822_m1
TaqMan Gene expression *Hmox1* Assay	Thermo-Fisher Scientific	Cat#Mm00516005_m1
TaqMan Gene expression *NOS2* Assay	Thermo-Fisher Scientific	Cat#Mm00440502_m1
TaqMan Gene expression *Sod1* Assay	Thermo-Fisher Scientific	Cat#Mm01344233_g1
TaqMan Gene expression *Cox2* Assay	Thermo-Fisher Scientific	Cat#Mm03294838_g1
TaqMan Gene expression *GAPDH* Assay	Thermo-Fisher Scientific	Cat#Mm99999915_g1